Geomech. Geophys. Geo-energ. Geo-resour. (2019) 5:171–196
https://doi.org/10.1007/s40948-018-00102-z

REVIEW

A review of mechanisms of induced earthquakes: from a view of rock mechanics

Jian-Qi Kang · Jian-Bo Zhu · Jian Zhao

Received: 7 January 2018 / Accepted: 17 December 2018 / Published online: 12 January 2019

Abstract The induced earthquake recently has gained an increasing public awareness of environmental and safety issue. The earthquakes associated with fluid injection and extraction, reservoir impoundment and mining/rock removal have been extensively reported. Here, we reviewed injection induced earthquakes and their mechanisms from a view of rock mechanics. This review begins by briefly introducing the classification and the state-of-the-art research of induced earthquakes. From a view of rock mechanics, three fundamental mechanisms of induced earthquakes, i.e., pore pressure increase, stress change, and change in coefficient of friction, are introduced in details. Firstly, we discussed pore pressure increase due to fluid injection and reservoir impoundment, and explained earthquakes caused by fluid injection and related to reservoirs according to the Mohr–Coulomb failure criterion and effective stress law in the saturated rock. Secondly, we discussed stress change resulting from fluid extraction, temperature change, reservoir loading and quarry unloading. Thirdly, we investigated factors determining coefficient of friction, i.e., mineralogy, fluid pressure and temperature. Moreover, it is a remarkable fact that additional physical or chemical effects of fluids may lead to weakening of materials in fault zones owing to stress corrosion and stable slip, according to the rate and state friction law. Finally, we summarized and compared mechanisms of induced earthquakes that occurred in a variety of past human activities and projects, and recommended future potential means and scopes to investigate the mechanism of induced earthquakes.

Keywords Induced earthquakes · Stress · Pore pressure · Friction coefficient

List of symbols

σ_θ	Tangential stress
σ_r	Radial stress
σ_1, σ_3	Axial stress
θ	Angle between the point on drilling wall and the σ_1 axis
$p_{initial}$	Pore pressure of the fracture opening initially
T_0	Tensile strength
k	Permeability coefficient
p	Pore pressure
c	Coefficient of consolidation
T'	Transmissivity
S	Coefficient of storage
q	Flow per unit width
J	Hydraulic gradient

J.-Q. Kang · J.-B. Zhu (✉)
State Key Laboratory of Hydraulic Engineering Simulation and Safety, School of Civil Engineering, Tianjin University, Tianjin, China
e-mail: jbzhu@tju.edu.cn

J. Zhao
Department of Civil Engineering, Monash University, Clayton, VIC, Australia

b	Distance between the parallel plate
v	Fluid kinematic viscosity
Q_{inject}	Volume of the injected fluid,
Q_{stored}	Total fluid volume stored in the fracture
Q_{lost}	Fluid volume lost into the surrounding aquifer
r_f	Half-length of the fracture
t	Time
q_I	Average rate of the injected fluid
C_L	Fluid-loss coefficient
h_f, w	Average fracture length and width
τ_{crit}	Critical shear stress
σ_n	Normal stress
μ	Coefficient of friction
C	Cohesion
α	Biot–Willis coefficient
v	Poisson's ratio
V	Reservoir volume
ρ	Density
c	Specific heat of the rock
T	Temperature
Q	Net flux out of heat out of the reservoir
μ_0	Coefficient of friction at a reference velocity (V_0)
V	Velocity
θ	State variable
dc	Critical displacement
a, b	Frictional parameters
K	Stiffness of the loading system
K_c	Critical fault stiffness
τ	Shear strength

1 Introduction

A great majority of earthquakes occurring each year around the world are natural ones. The rest seismic events that are small in magnitudes are related to human activities and called "induced seismic events" or "induced earthquakes" (National Research Council 2012). Induced earthquakes in connection with human activities were observed as early as in 1920s, and recently, they have attracted increasing public concerns about environmental and safety issues in the world. Human activities potential to induce earthquakes encompass the impoundment of water reservoir (Ying 2010), fluid injection (Raleigh et al. 1972; Seeber et al. 2004), fluid extraction in the oil and gas industry (Segall 1989; Grasso 1992; Segall et al. 1994; Davies et al. 2013), mining/rock removal (McGarr 1976; Richardson and Jordan 2002), enhanced geothermal systems (EGS) (Feng et al. 2014; Deichmann et al. 2014), and cavity collapses as a result of underground nuclear explosions (Boucher et al. 1969). In accordance with the proportion of stress change and energy caused by human activities, McGarr and Simpson (1997) classified earthquakes related to human activities into two types, i.e., "triggered earthquakes" and "induced earthquakes". Since it is rarely possible to reliably quantify the human-related stress change, the distinction between induced and triggered earthquakes is difficult. Hence, the term "induced earthquakes" is used in this paper.

More and more induced earthquakes are documented during the past 100 years. Earthquakes whose magnitudes are greater than 6 occurred in Hsinfengkiang, China in 1962, Kariba, Zambia–Zimbabwe Border in 1963, Kremasta, Greece in 1966 and Koyna, India in 1967. So far, the greatest reservoir induced earthquake is the 6.3-magnitude earthquake in Koyna (Gupta 2002). The greatest earthquake potentially related to fluid injection, an Mw 5.7 one, happened in November 2011 in Oklahoma, USA (Keranen et al. 2013), which was felt in at least 17 states of USA and caused damage in the epicentral region. An Mw 5.4 mining-induced earthquake occurred at a depth of about 900 m in Völkershausen, German in 1989 (Grünthal 2014). These above great-magnitude earthquakes resulted in huge losses of life and property.

In addition to great induced earthquakes, there exist more lesser ones. Although they are too small to cause huge damage to life and property, they could draw great attentions or even panics from the society if close to residential areas. For example, during the EGS project in Basel, Switzerland, a cluster of earthquakes of magnitude up to 3.4 occurred between December 2006 and March 2007, which resulted in the cancellation of the project in December 2009 (Deichmann and Giardini 2009).

Therefore, it is of great academic interest and practical significance to investigate and understand the mechanisms of induced earthquakes, so as to predict and assess the potential risks.

Many studies have been performed on the mechanisms of induced earthquakes. The earthquakes at the Rocky Mountain Arsenal, USA in 1960s were

believed to arise from fluid pressure increase (Van Poollen and Hoover 1970). Weingarten et al. (2015) suggested that the magnitude of induced earthquakes depend on injection rates. Keranen et al. (2014) pointed out that the increase in overpressure zones in Oklahoma potentially accounts for the largest swarm. Segall and Lu (2015) analyzed the relationship between pore pressure and seismicity rates considering hydro-mechanical coupling and time-dependent earthquake nucleation. Van Wees et al. (2014) claimed that induced seismicity associated with gas field depletion is attributed to differential compaction. Guglielmi et al. (2015) reported that most aseismic slip occurs within the fluid-pressurized zone and obeys a velocity strengthening friction law. McClure and Horne (2011) proposed the sequential stimulation (SS) mechanism to explain the phenomenon that the failure zone grows during fluid injection into a single isolated fracture. Jeanne et al. (2014) conducted a series of 3D simulations to study the effects of thermo-hydro-mechanical (THM) processes on the EGS. De Simone et al. (2013) identified that hydraulic stimulation and geothermal reservoir operation may disturb the rock mechanical stability and trigger micro-seismic events.

This paper presents a detailed review of the mechanisms of induced earthquakes from a view of rock mechanics. This review includes six sections. Section 2 presents hydraulic fracturing, the Mohr–Coulomb failure criterion and effective stress law in the saturated rock, and discusses pore pressure increase due to fluid injection and reservoir impoundment. Section 3 discusses stress change resulting from factors including fluid extraction, temperature change, reservoir loading and quarry unloading. In Sect. 4, firstly, the rate and state friction law is introduced; subsequently, some factors, i.e., mineralogy, fluid pressure and temperature, influencing coefficient of friction are summarized; finally, additional physical or chemical effects of fluids leading to weakening of materials in fault zones owing to stress corrosion and stable slip are described with the rate and state friction dependent law. In Sect. 5, mechanisms of induced earthquakes that occurred in variety of past human activities and projects are summarized and compared. In Sect. 6, the three mechanisms are often coupled and occur at the same time, e.g., fluid injection changes pore pressure, stress and coefficient of friction. And future potential means and scopes to investigate the mechanism of induced earthquakes are recommended.

2 Pore pressure increase

2.1 Hydraulic fracturing

Hydraulic fracturing has been widely applied to improve the efficiency of geothermal reservoir, gas and oil secondary recovery, and liquid waste disposal, through increasing fractures in the low-permeability formation. During hydraulic fracturing, earthquakes are induced attributed to two mechanisms, i.e., hydraulic fracture opening and the approximately linear diffusion of the fluid (Wolhart et al. 2005; Vulgamore et al. 2007; Maxwell et al. 2008; Cipolla et al. 2012).

Based on the theory of elastic mechanics, when the drilling is located in a two-dimensional stress field (σ_1, σ_3) in an infinite body, the rock in a distance from the drilling end is in a plane strain state. Stresses on the drilling wall are:

$$\begin{aligned} \sigma_\theta &= \sigma_1 + \sigma_3 - 2(\sigma_1 - \sigma_3)\cos 2\theta \\ \sigma_r &= 0 \end{aligned} \tag{1}$$

where σ_θ is the tangential stress and σ_r is the radial stress, θ is the angle between the point on the drilling wall and the σ_1 axis. When $\theta = 0^\circ$ or 180°, the minimal value of σ_θ follows

$$\sigma_\theta = 3\sigma_3 - \sigma_1 \tag{2}$$

As shown in Fig. 1, when the pressure exceeds the sum of $3\sigma_3 - \sigma_1$ and the tensile strength (T_0) of rock, tensile cracks will be generated. The tensile crack initiates on the drilling wall where $\theta = 0^\circ$ and 180°, and propagates in a direction parallel to σ_1. The pore pressure ($p_{initial}$) of the fracture opening initially equals:

$$p_{initial} = 3\sigma_3 - \sigma_1 + T_0 \tag{3}$$

The length and number of fractures around the drilling increases with increasing pore pressure, injection volume and injection rate. The tensile fracture releases less kinetic energy than that caused by shearing. In general, the magnitude of induce earthquakes related to the hydraulic fracturing is small.

Hydraulic fracturing can result in not only tensile damage but also shear damage of rock by increasing pore pressure on faults around the injection well, as illustrated in Fig. 2. This can be interpreted with

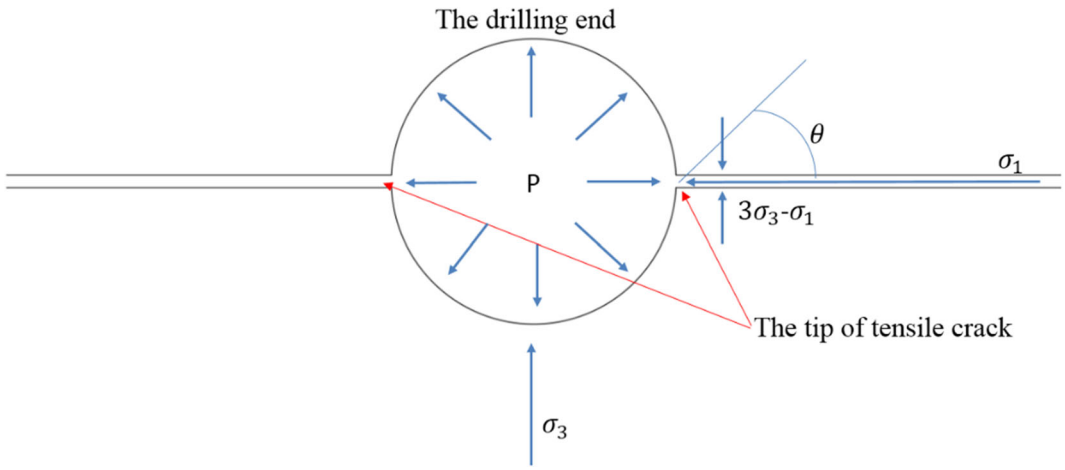

Fig. 1 Schematic diagram illustrating the hydraulic fracturing. When the pressure (P) exceeds the sum of $3\sigma_3 - \sigma_1$ and the tensile strength (T) of rock, the tensile crack initiates on the drilling wall where $\theta = 0°$ and $180°$

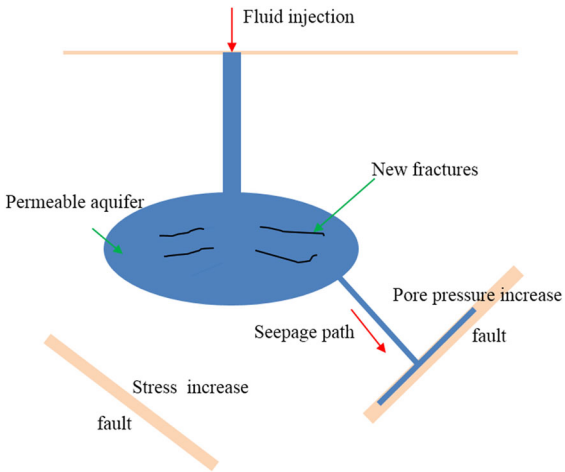

Fig. 2 Schematic diagram illustrating injection induced earthquakes. The right fault slip is caused by increasing the pore pressure on the fault. The left fault slip is caused by additional stress from the increasing volume of the permeable aquifer

Mohr–Coulomb failure criterion and effective stress law that are detailly described in the following section. The induced 5.0-magnitude earthquake in November 2011 in Oklahoma, USA is potentially associated with pore pressure increase after hydraulic fracturing and has a late response to the fluid injection (Keranen et al. 2013).

The late occurrence of induced earthquakes in the process of fluid injection could be explained by pressure diffusion. Darcy's law is among the earliest solutions of pressure diffusion (Biot 1941):

$$v_x = k\frac{\partial p}{\partial x}, v_y = k\frac{\partial p}{\partial y} \tag{4}$$

where k is permeability coefficient, p is the pore pressure.

Assuming that the fluid is incompressible, the fundamental seepage equation of steady flow in a two-dimensional plane is:

$$\frac{\partial^2 p}{\partial x^2} + \frac{\partial^2 p}{\partial y^2} = 0 \tag{5}$$

Terzaghi (1923) derived the seepage equation of unsteady flow for one-dimensional consolidation:

$$\frac{\partial p}{\partial t} = c\frac{\partial^2 p}{\partial z^2} \tag{6}$$

where c is coefficient of consolidation.

Based on the concept of aquifer, Jacob (1940) proposed diffusion equation for two-dimensional flow in a confined aquifer:

$$\frac{\partial p}{\partial t} = \frac{T'}{S}\left(\frac{\partial^2 p}{\partial x^2} + \frac{\partial^2 p}{\partial y^2}\right) \tag{7}$$

where T' is transmissivity, S is the coefficient of storage.

The above equations were derived under the precondition of fluid flow in the porous medium. On the contrary, rock mass is generally composed of intact rock and fractures. The intact rock can be treated as the porous medium. However, the fluid flow in the rock fracture is different from that in the porous

medium. Seepage behaviors of fluid are determined by the properties of rock fracture, e.g., the fracture's aperture. According to Navier–Stokes equation, fracture flow through parallel plates is given by:

$$q = \frac{gb^3 J}{12v} \tag{8}$$

where q is flow per unit width, J is the hydraulic gradient, b is the distance between the parallel plate, v is fluid kinematic viscosity.

Fracture growth and pressure diffusion exist in the whole processes of hydraulic fracturing. When pressure in the pre-existing fracture is higher than $p_{initial}$, microearthquakes are mainly caused by fracture growth. Shapiro et al. (2006) proposed an equation of the fracture growth, which is given by

$$Q_{inject} = Q_{stored} + Q_{lost}, r_f(t) = \frac{q_I t}{2h_f w + 4h_f C_L \sqrt{2t}} \tag{9}$$

where Q_{inject} is the volume of the injected fluid, Q_{stored} is the total fluid volume stored in the fracture, Q_{lost} is the fluid volume lost into the surrounding aquifer, r_f is the half length of the fracture and treated as a function of the injection time t, q_I is the average rate of the injected fluid, C_L is the fluid-loss coefficient determined by many factors such as the injection pressure and the hydraulic diffusivity of the rock, h_f and w are the average fracture length and width, respectively.

Based on Eq. (9), the length of fractures increases with increasing injected fluid and increasing time. This could enhance the seepage capability of the rock formation. Meanwhile, hydraulic fracturing can also change the stress condition surrounding the rock formation, e.g., the neighboring pre-existing fault (Rutledge and Phillips 2003).

If the pressure in the pre-existing fracture is lower than $p_{initial}$, the pressure diffusion dominates the features of induced earthquakes. Treating fluid injection in a borehole as a point source of pore pressure perturbation, Shapiro and Dinske (2009) proposed the "triggering front" and "back front" concepts that can describe the spatial and temporal behaviors of induced earthquakes related to pressure diffusion in the infinite, hydraulically isotropic and homogeneous saturated rock. As illustrated in Fig. 3, induced earthquakes occur between the "triggering front" and "back front".

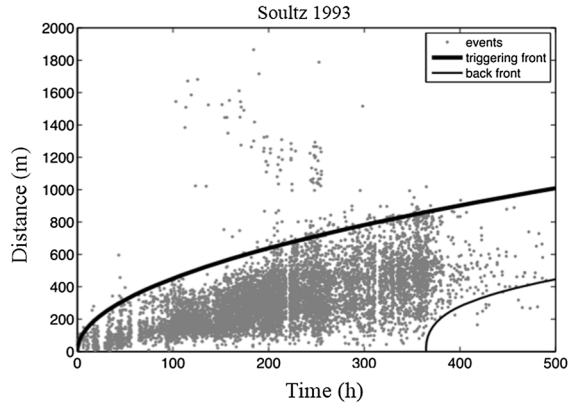

Fig. 3 Induced microseismic events at a borehole in Soultz, France. The thick line is "triggering front", and the thin line is "back front". Induced earthquakes occur between the 'triggering front' and 'back front'. Adapted after Shapiro and Dinske (2009)

2.2 Mohr–Coulomb failure criterion

Different from hydraulic fracturing resulting in tensile failure of rock, with increasing pore pressure, shear failure could happen on the fault (Atkinson et al. 2016; Ellsworth 2013; Keranen et al. 2013). At present, the Mohr–Coulomb failure criterion and effective stress law in the saturated rock can explain the shear failure. The Mohr–Coulomb failure criterion is shown as follows (Jaeger and Cook 1979):

$$\tau_{crit} = C + \mu(\sigma_n - P) \tag{10}$$

where τ_{crit} is the critical shear stress loading on a fault and results in fault slip,σ_n is the normal stress acting across the fault, C is cohesion and μ is the coefficient of friction.

Based on Eq. (10), the shear strength of faults decreases with increasing pore pressure. As shown in Fig. 4a, when the pore pressure increases to the critical pressure, the solid circle moves to the failure curve and is tangent to the failure curve. This indicates that induced earthquakes occur on the normal fault due to the reduction in shear strength, as shown in Fig. 4b.

3 Stress change

3.1 Stress change due to fluid extraction

After fluid extraction, pore pressure decreases and the pore in the reservoir rock could be compressed and

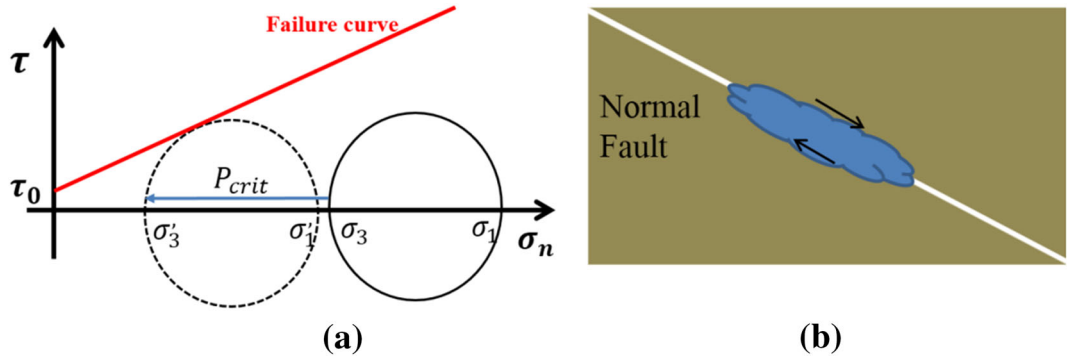

Fig. 4 Schematics of Mohr–Coulomb failure criterion. **a** The Mohr circle and failure curve. The solid circle moves towards the failure curve with increasing pore pressure. When the solid circle is tangent to the failure curve and becomes a dotted circle, the pore pressure increases to the critical pressure and the shear strength decreases to the limited strength. **b** Schematic diagram illustrating normal fault. The reduction in shear strength on the fault can cause induced earthquakes

closed. This produces static stress and may reactivate the fault in the critical failure state. Segall (1989) suggested that the normal and reverse fault slips around the reservoir are attributed to stress change due to fluid extraction. Santarelli et al. (1998) pointed out the importance of changes in pressure during depletion known as the reservoir stress path. Hillis (2000) and Tingay et al. (2003) used pore pressure/stress coupling to explain the phenomenon of the reduction in σ_h with decreasing pore pressure in hydrocarbon reservoirs. This is also known as stress depletion response of the reservoir (Addis 1997). "pore pressure/stress coupling" can be expressed by the ratio $d\sigma_h/d_p$, which describes the change in total minimum horizontal stress caused by the change in pore pressure. Analytically, Engelder and Fischer (1994) derived a space- and time-independent expression for the ratio $d\sigma_h/d_p$ under four assumptions, i.e., a horizontal infinitely large reservoir, constant vertical initial stress which does not change laterally or with changing pore pressure, uniaxial strain condition with horizontal strains equal to zero, and equal changes in the maximum and the minimum horizontal stresses. The ratio $d\sigma_h/d_p$ is given by (Engelder and Fischer 1994):

$$\frac{d\sigma_h}{dp} = \alpha \frac{1-2v}{1-v} \tag{11}$$

where α is Biot–Willis coefficient, v is the Poisson's ratio.

Hydraulic fracturing measurement shows that minimum horizontal stresses decrease (become more tensile) with decreasing reservoir pore pressure (Addis 1997). The value of $d\sigma_h/d_p$ is summarized in Table 1.

As shown in Fig. 5, when the fluid is extracted completely, the rock is in compressional or extensional environments. The normal fault may be reactivated in the extensional environments. The reverse fault may be reactivated in the compressional environments.

3.2 Stress change due to temperature change

Production from geothermal reservoirs in saturated conditions could result in a decline in reservoir temperature in addition to decreased pressure (Ernest et al. 2007). Interaction between cool fluid and hot rock causes contraction of fracture surfaces, known as the thermoelastic strain. The thermal contraction can create fractures and seismicity.

Segall and Fitzgerald (1998) used an energy conservation equation to estimate the average temperature change of geothermal reservoir and obtained the stress change. This equation was derived from a net energy balance of geothermal energy and based on the condition that thermal energy is contained within the solid phase:

$$\mathrm{V}\rho c \frac{dT}{dt} = -Q \tag{12}$$

where V is the reservoir volume, ρ is the density, c is specific heat of the rock, T is temperature, and Q is the net flux out of heat out of the reservoir.

Assuming that the system is at steady state prior to geothermal production, Segall and Fitzgerald (1998) found that the cooling rate ($\frac{dT}{dt}$) is $-0.3^{\circ}\mathrm{C}/\mathrm{year}$, i.e., a net temperature decline of 6 °C over 20 years, which

Table 1 The values of $d\sigma_h/d_p$

Area	Scale	$\Delta\sigma_h/\Delta P$	References
Scotian Shelf, Canada	Basin (overpressure)	0.76	Bell (1990)
Vicksburg Formation, South Texas	Field (depletion)	0.48	Salz (1977)
Travis Peak Formation, East Texas	Field (depletion)	0.57	Whitehead et al. (1987)
Alberta Basin, Western Canada	Field (depletion)	0.34	Woodland and Bell (1989)
Ekofisk Field, North Sea	Field (depletion)	~0.8	Teufel et al. (1991)
US Gulf Coast	Basin (overpressure) & field (depletion)	0.46	Breckels and van Eekelen (1982)
Lake Maracaibo, Venezuela	Field (depletion)	0.56	
Brunei	Basin (overpressure) & field (depletion)	0.49	
Magnus Field, North Sea	Field (depletion)	0.68	Addis (1997)
West Sole Field, North Sea	Field (depletion)	1.18	
Wytch Farm Field, UK	Field (depletion)	0.65	
Venture Field, Canada	Basin (overpressure)	0.56	

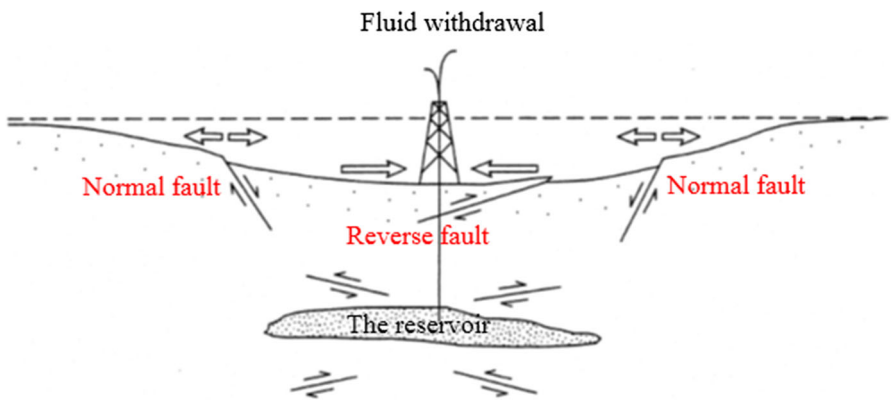

Fig. 5 Summary of observed faulting associated with fluid withdrawal. When the fluid is extracted, the normal fault and reverse fault can be reactivated beside and above the reservoir, respectively. Adapted after Segall (1989)

is sufficient to generate significant thermoelastic stresses, i.e., a stressing rate of 0.09 MPa/year. Stress changes of this magnitude can induce earthquakes in the critically stressed crust.

The temperature change within the reservoir is extremely non-uniform, with great concentrations near injection wells and steam-producing fractures. Mossop and Segall (1997) showed that thermoelastic stresses generated from injection of cold fluids into hot rock are quite appreciable. Segall and Fitzgerald (1998) illustrated that thermoelastic stressing cannot be ignored in geothermal reservoirs and is quite likely the dominant effect in altering the stress state within the reservoir. This indicates that microseismicity within the Geysers, USA reflects temperature changes and may be useful in monitoring cold injection within the reservoir. Therefore, THM modeling was performed for cold water injection into a planar fracture (Kohl et al. 1995; Ghassemi et al. 2008; Ghassemi and Zhou 2011) or into a fracture network (Kolditz and Clauser 1998; Bruel 2002; McDermott et al. 2006). De Simone et al. (2013) analyzed the thermoelastic effects on the rock within and surrounding a fracture zone. They performed 2D coupled THM and hydro-mechanical (HM) simulations, and their results showed that thermal effects induce significant thermal stress perturbation in the surrounding intact rock.

As an example, Fig. 6 displays the stress state at three locations that are 3 m away from the injection well, i.e., Point A inside the fracture, Point B at the interface between the fracture and the matrix, and Point C inside the matrix and 0.4 m away from interface (De Simone et al. 2013). Results of the HM

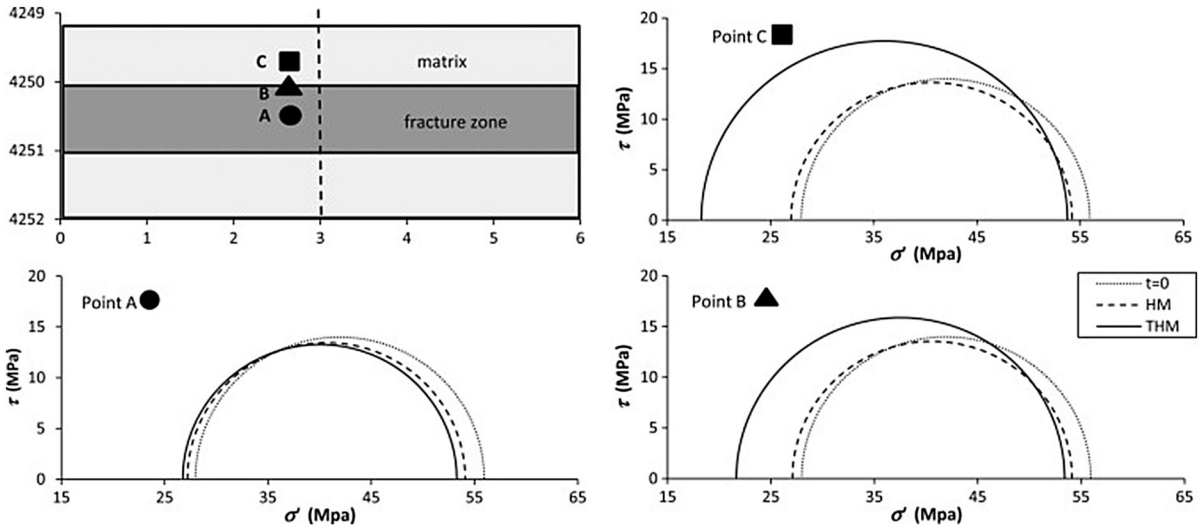

Fig. 6 Changes in effective stress at points placed 3 m away from the injection well at different depths. The solid line represents the THM solution, the dashed line represents the HM solution, and the dotted line indicates the initial situation (De Simone et al. 2013)

simulation show that the vertical effective stress decreases more than the horizontal one. This produces smaller Mohr circles. In the case of the THM simulation, the thermal contraction causes an increase of the deviatoric stress in the cooled section of the matrix, which results in larger Mohr circles at Points B and C. Note that the Mohr circle size is greater at Point C, reflecting a more critical situation. Inside the fracture zone, i.e., Point A, the results of THM and HM simulation are similar, indicating a more stable condition.

3.3 Stress change due to reservoir loading and quarry unloading

The impoundment of a large reservoir can change rock stress around the reservoir, which could induce earthquakes (Bell and Nut 1978; Simpson 1986; Yi et al. 2012). Unloading stress from quarry unloading could control the shallow fault slip (Yerkes et al. 1983; Porsani et al. 2006). The effects of reservoir loading and quarry unloading on the frictional strength are shown in Fig. 7. In quarrying operation, the vertical load is reduced. This may induce earthquakes in the thrust fault environment (Fig. 7a). On the contrary, reservoirs impound and blasting enhance the vertical load, which may induce earthquake for the normal fault (Fig. 7b).

3.4 Stress change in underground mines

Because of excavation of large volumes of rocks in underground mines, stress change could result in fracture initiation, propagation and fault slip close to underground mines, which usually generate seismic waves. Figure 8 shows four mining induced seismicities and seismic waves (Horner and Hasegawa 1978) and dynamical loading, i.e., seismic waves, could result in fault slip far from underground mines. The mechanisms of mining induced seismicity include the sudden release of elastic strain energy in rock mass due to stress concentration, and fault slip due to mining-induced stress change including dynamic loading as shown in Fig. 8.

4 Change in coefficient of friction

A detailed introduction of the behaviors of fault slip is provided in this section, taking account of the influence of the mineralogy, fluid pressure, temperature and sliding velocity, and a summary of the corresponding results is presented. In addition, the chemical effect of fluid on the rock strength is described.

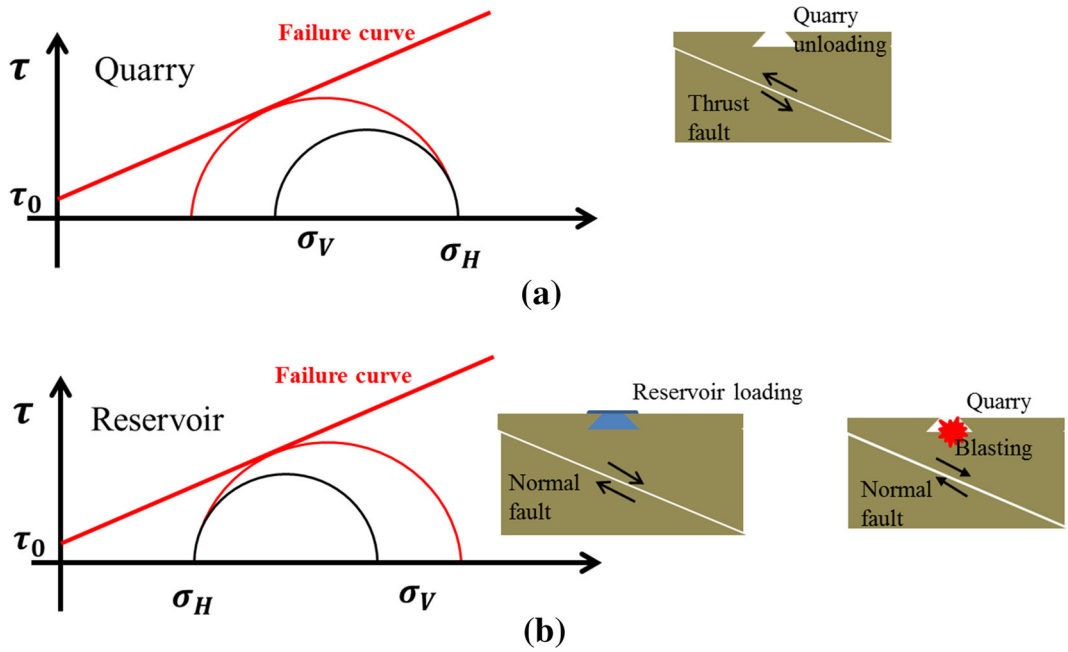

Fig. 7 The Mohr circles showing the fault slip attributed to stress change

4.1 The rate and state friction law

Mohr–Coulomb failure criterion and effective stress law were traditionally adopted to understand the mechanisms of induced earthquakes, with which, influences of fluid pressure, temperature or stress change on fault reactivation could be well explained. However, it is difficult for them to describe the whole fault slip process and to address the question whether seismic or aseismic slip happens after fault reactivation.

Based on experimental studies of rock friction, a set of constitutive equations, defined as the rate and state friction laws, has been proposed (Dieterich 1978; Ruina 1983):

$$\mu = \mu_0 + a \cdot \ln(V/V_0) + b \cdot \ln(V_0 \cdot \theta/d_c) \tag{13}$$

$$\frac{d\theta}{dt} = 1 - \frac{\theta \cdot V}{dc} \tag{14a}$$

or

$$\frac{d\theta}{dt} = -\frac{V\theta}{dc}\ln\left(\frac{V\theta}{dc}\right) \tag{14b}$$

where μ (coefficient of friction) is the shear stress divided by the effective normal stress acting on the fault, μ_0 is the coefficient of friction at a reference velocity (V_0), V is velocity, θ is the state variable. The characteristic or critical displacement dc is the sliding distance at a constant V, through which the surface in contact changes. a and b are parameters characterizing the effect on fault slip, as illustrated in Fig. 9.

The friction at the steady state velocity is (Scholz 2002):

$$\mu = \mu_0 + (a - b) \cdot \ln(V/V_0) \tag{15}$$

This law can provide a more comprehensive interpretation of the phenomenon of the coefficient of friction changing with slip velocity and other factors, and decide whether seismic or aseismic slip is induced by fluid pressure, temperature, or stress change.

As shown in Fig. 9, if $a - b > 0$, the fault is velocity strengthening, i.e., the friction increases with the slip velocity, and the fault slip is intrinsically stable. In contrast, if $a - b < 0$, the fault is velocity weakening, which means the fault slip exhibits conditional stable behavior or unstable characteristics, depending on the elastic stiffness of the loading system K and the critical fault stiffness K_c. K_c depends on the effective normal stress and the frictional parameters of the fault (Scuderi and Collettini 2016):

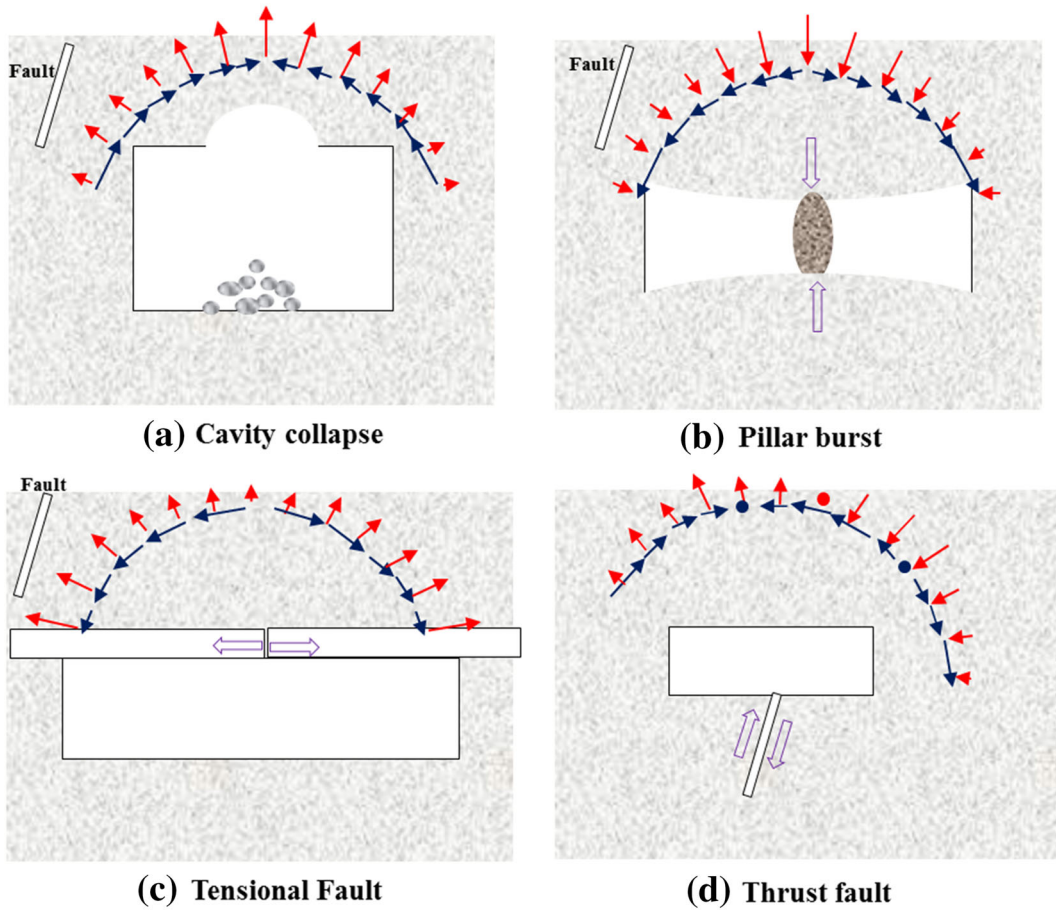

Fig. 8 Schematic diagram of four possible ways in mining induced seismicity. Purple arrows indicate mining induced force direction. Red arrows and blue arrows indicate normalized far-field P-wave and S-wave, respectively (after Horner and Hasegawa 1978)

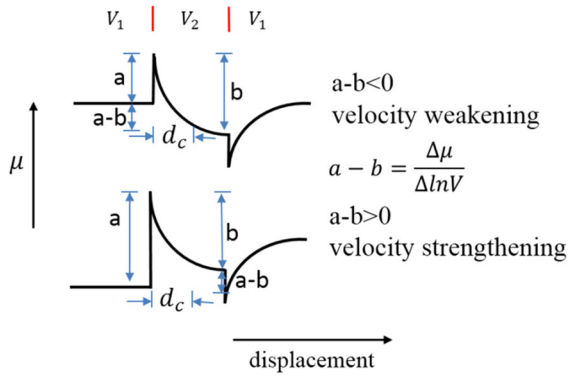

Fig. 9 Schematic diagram showing the parameters in the rate and state friction laws and the frictional parameters (a − b)

$$K_c = \frac{(b-a)*(\sigma_n - P)}{d_c} \tag{16}$$

When $K > K_c$, the resistance to fault slip decreases slower than the elastic unloading related to fault slip, and the fault favors stable sliding, i.e., aseismic slip, and vice versa. Equation (16) could further explain fault slip with velocity-strengthening frictional behavior. When a − b > 0 (i.e. $K_c < 0$), and $K > 0$, the fault keeps stable slip until new induced factors emerge. Therefore, the frictional parameter (a − b) plays an important role in the fault frictional stability. (a − b) depends on the mineralogy, fluid pressure, temperature and sliding velocity (Ikari et al. 2007; Rutqvist et al. 2008; Scuderi and Collettini 2016).

4.1.1 *Effect of mineralogy on frictional parameter (a − b)*

There is a common assumption that the great majority of earthquakes happen on the strong fault with large coefficient of friction and the aseismic slip occurs on the weak fault (Scholz 2002), with which, extensive studies have been conducted (Shimamoto and Logan 1981; Morrow et al. 2000; Ikari et al. 2007, 2009, 2010; Niemeijer and Collettini 2013). They suggested that the mineral of fault gouge controls the frictional strength as well as fault slip. These experiments revealed that (a − b) is attributed to the fault strength, i.e., the initial coefficient of friction.

Summarizing previous studies of friction of all kinds of crystalline and quartzo-feldspathic rock, Byerlee (1978) achieved the following fitting equations:

$$\begin{aligned} \tau &= 50 + 0.6\sigma_n, \sigma_n > 200\,\text{MPa} \\ \tau &= 0.85\sigma_n, \sigma_n \leq 200\,\text{MPa} \end{aligned} \tag{17}$$

The maximum coefficient of friction is constant, i.e., $\mu = 0.6$ (when $\sigma_n > 200\,\text{MPa}$) and $\mu = 0.85 (\sigma_n \leq 200\,\text{MPa})$. The shear strength of faults is usually proportional to the coefficient of friction. Whereas, fault gouges containing phyllosilicate exhibit notably lower coefficient of friction. In particular, montmorillonite with high absorption performance in water has a coefficient of friction of only 0.18 under the normal stress of 20 MPa at room temperature (Ikari et al. 2010). The coefficient of friction of different kinds of gouges during steady sliding is shown in Fig. 10a. Fault gouges composed of halite, talc, montmorillonite and biotite exhibit low frictional strength ($\mu < 0.4$) (Byerlee 1978; Shimamoto and Logan 1981; Ikari et al. 2010). In contrast, fault gouges with rich silicate or carbonatite mineral (quartz, westerly granite, orthoclase, calcite, dolomite and limestone) have a large friction coefficient ($\mu > 0.5$) (Shimamoto and Logan 1981; Carpenter et al. 2009; Ikari et al. 2010). The friction coefficient of fault gouges composed of phyllosilicate is between 0.35 and 0.5 (Ikari et al. 2010).

Fault gouges are essential for fault slip. In specific, fault slip depends on the initial coefficient of friction which depends on fault gouges. Byerlee and Brace (1968) found that fault gouges with rich strong minerals exhibit more unstable sliding than those with rich weak mineral. Summers and Byerlee (1977) claimed fault gouges containing strong and brittle minerals, e.g., quartz or feldspar, facilitate fault unstable slip. Shimamoto and Logan (1981) conducted experiments for monomineralic gouges and suggested that Mohs' hardness of a mineral plays an important role on the analysis of fault slip. In term of mineralogy, the fault with low strength has a trend of velocity-strengthening and (a − b) increases with increasing phyllosilicate content (Morrow et al. 2000; Moore 2004; Ikari et al. 2007; Carpenter et al. 2009; Tembe et al. 2010; Boulton et al. 2012; Niemeijer and Collettini 2013). Ikari et al. (2010) conducted a large number of laboratory experiments and confirmed a systematic relationship between friction strength and the behavior of fault slip. Notably, the fault slip evolves from velocity strengthening to velocity weakening or keeps velocity strengthening with increasing coefficient of friction (Fig. 10b). When $\mu < 0.5$, the fault exhibits aseismic slip. The fault gouge with coefficient of friction greater than 0.5 exhibits seismic slip or conditional stability. However, some gouges composed of phyllosilicate (Serpentinite, 50% Kaolinite 50% Quartz, Kaolinite) exhibit velocity weakening and strain hardening under loading, which dramatically improves the fault strength. An explanation of mineralogy dependence of (a − b) is that the platy characteristic of phyllosilicate mineral increases the contact area, suppresses change of the contact area, and hence decreases the value of b (the evolution effect) (Ikari et al. 2010).

4.1.2 *Effect of fluid pressure on frictional parameter (a − b)*

As mentioned in Sect. 2, increasing fluid pressure can reactivate the fault and induce earthquake, i.e., fault unstable slip, by reducing the effective normal stress on the fault. This has been supported by the positive correlation between fluid diffusion and the spatio-temporal evaluation of induced earthquakes (Shapiro et al. 2006, Shapiro and Dinske 2009). However, recent studies implied that fluid pressure could also result in aseismic slip, i.e., fault stable slip. Aseismic slip events occur at a zone of high fluid pressure in the subducting oceanic crust (Kodaira et al. 2004). The fault slips aseismically on the fluid overpressure domains, defined as high V_p/V_s zones (Moreno et al.

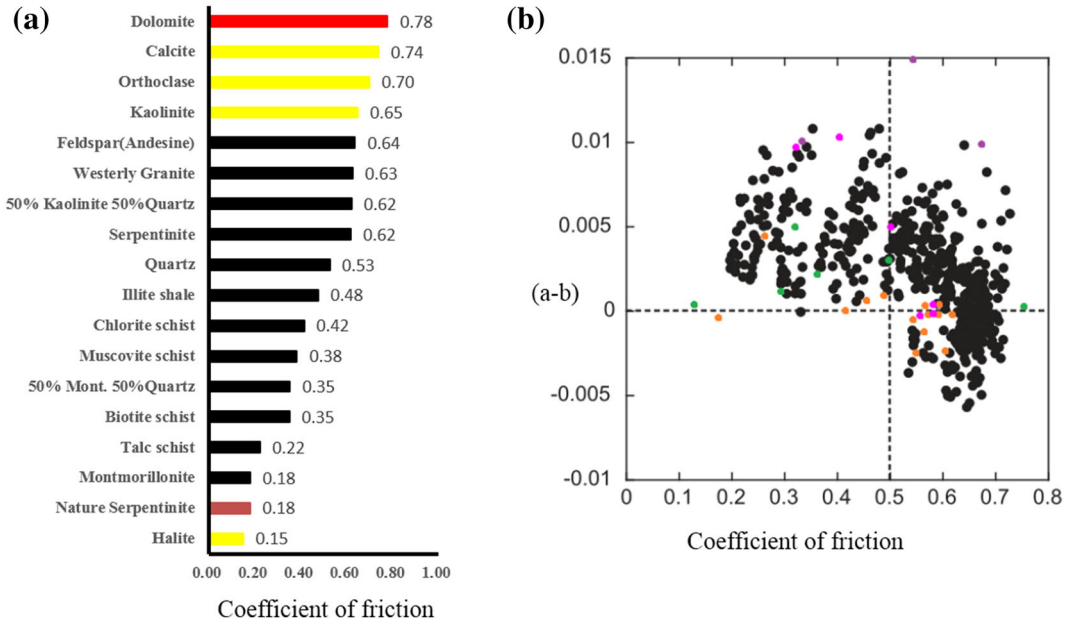

Fig. 10 Summaries of coefficient of friction. **a** The coefficient of friction versus rock minerals. **b** The coefficient of friction dependence of frictional parameter (a − b) adapted after Ikari et al. (2009). The data are taken from Byerlee (1978) (Red), Shimamoto and Logan (1981) (Yellow), Carpenter et al. (2009) (Orange), Ikari et al. (2010) (Black), Tembe et al. (2010) (Green), Boulton et al. (2012) (Pink), Niemeijer and Collettini (2013) (Purple), and Kohli and Zoback (2013) (Gray)

2014). Guglielmi et al. (2015) proposed that fluid injection stimulates aseismic slip and micro-earthquakes subsequently result from aseismic creep by fluid injection test on a preexisting fault. Scuderi and Collettini (2016) conducted laboratory experiments and concluded that the pore fluid pressure controls the fault slip and facilitates fault stable slip. De Barros et al. (2016) asserted that the presence of fluid and calcite gouges on the fault suppresses the unstable slip. The fluid pressure gives rise to seismic slip as well as aseismic slip.

However, how to interpret this obvious contradiction is a challenging work. Many studies have been performed to explain the role of fluid pressure on the fault slip based on the rate and state friction law. Ikari et al. (2007) found that (a − b) increases with water content increasing from 0 to 20% at shear velocity steps between 100 μm/s and 300 μm/s. Guglielmi et al. (2015) injected fluid into a natural fault and measured fault slip, and found that most slip exhibit velocity strengthening with a − b = 0.045.

There are two mechanisms for fluid pressure to stimulate aseismic slip. One is K_c reduction derived from increasing fluid. Equation (9) predicts that K_c decreases with increasing fluid pressure, and the fault favors stable slip (Scholz 1998). However, Scuderi and Collettini (2016) suggested that the frictional parameter (a − b) remains positive and decreases with increasing fluid pressure, but exhibits velocity neutral behavior in a near lithostatic fluid pressure condition (shown in Fig. 11). The other mechanism is that shear dilation inhibits seismicity (Yamashita 1999, Segall et al. 2010). Pore volume dilation occurs with the fault slip (Marone et al. 1990). The permeability of fault with clay rich gouges is low. When this fault with fluid pressure is reactivated, the permeability increases with pore volume dilation resulting from fault slip. This can lead to the reduction of fluid pressure and increase of the effective stress loading on the fault, which can increase the frictional strength and result in stable slip

4.1.3 Effect of temperature on frictional parameter (a − b)

Temperature is an important factor that influences the frictional strength and slip behaviors of faults. To understand the mechanism of the effect of temperature on the fault slip behavior, extensive laboratory experiments have been conducted in different conditions

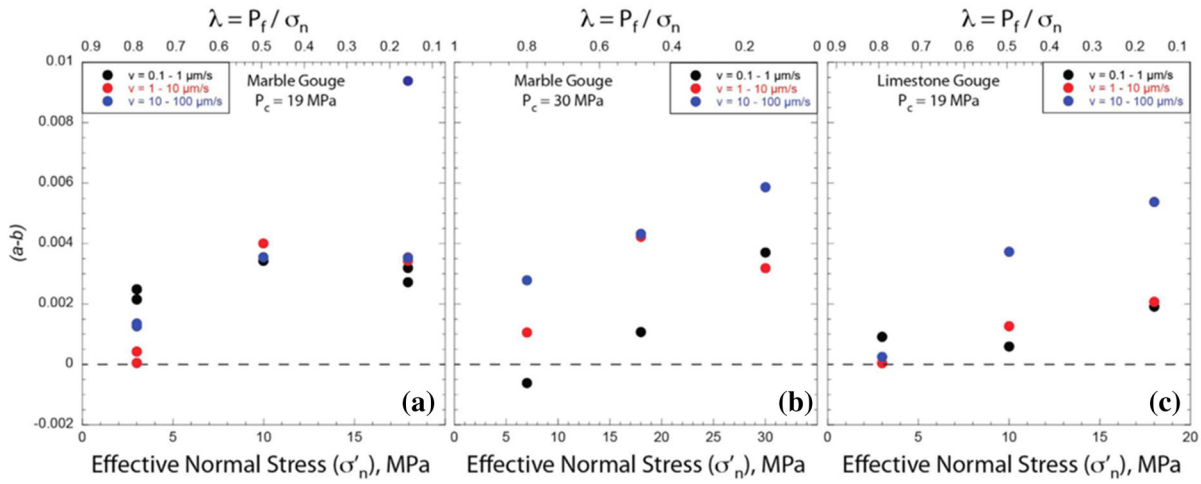

Fig. 11 The frictional parameters (a − b) as a function of fluid pressure. (a − b) evolves from velocity strengthening to velocity neutral behavior with increasing fluid pressure (Scuderi and Collettini 2016)

(Rutqvist et al. 2008; Verberne et al. 2010; Den Hartog et al. 2012a, b; Niemeijer and Collettini 2013; McClure and Horne 2014; Verberne et al. 2015; He et al. 2016). Blanpied et al. (1995) suggested that the friction coefficient is 0.7–0.8 below 250 °C and decreases dramatically with increasing temperature for wet granite, and predicted that the depth of evolution from velocity strengthening to velocity weakening is 13 km. He et al. (2006) conducted experiment at elevated temperatures up to 615 °C and inferred that fault gouges may exhibit velocity weakening at above 420 °C and at least up to 615 °C. The effect of temperature on the frictional strength and slip behaviors of faults is summarized in Figs. 12 and 13. The main mechanism for changing (a − b) may be that the fault gouges evolve from semi-brittle/frictional to plastic deformation behavior.

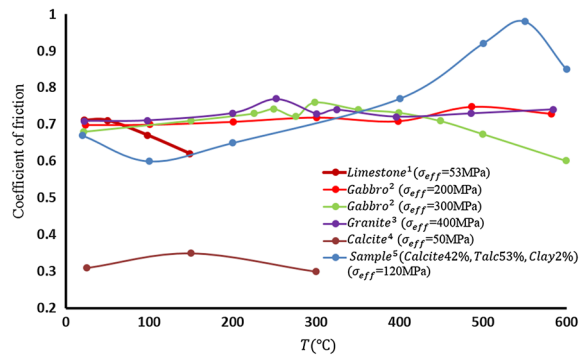

Fig. 12 Coefficient of friction at steady state as a function of temperature. Data of limestone was obtained at a shear velocity of 1.22 μm/s (Verberne et al. 2010). Data of gabbro was generated at the same shear velocity above (He et al. 2007). Data of granite was generated at a shear velocity of 1.15 μm/s (Blanpied et al. 1995). Data of calcite was obtained using a shear velocity of 1 μm/s (Verberne et al. 2015). Data of sample (calcite 42%, talc 53%, clay 2%) was generated at a shear velocity 10 μm/s (Niemeijer and Collettini 2013)

4.2 Chemical effects of fluid

4.2.1 Decrease of friction coefficient

Recent studies suggested that fluid can influence the frictional strength as well as the slip behaviors of the fault by changing coefficient of friction, as observed in the field and laboratory tests (Moore 2004; Ikari et al. 2007; Okazaki et al. 2013; Kawai et al. 2015). Schulz et al. (1983) suggested that creep events happening on the San Andreas fault are related to rainfall which softens the fault gouges, and these creep events are smaller and occur earlier than those during the dry season.

Laboratory experiments examining the influence of fluid on the fault minerals have also been carried out (Moore 2004; Ikari et al. 2007; Okazaki et al. 2013; Kawai et al. 2015). The average coefficient of friction of fault gouges under dry and wet condition is summarized in Table 2. When fault gouges change from dry to wet conditions, the decrease percentage of μ is shown in Fig. 14. The decrease percentage of the friction coefficient of fault gouges composed of

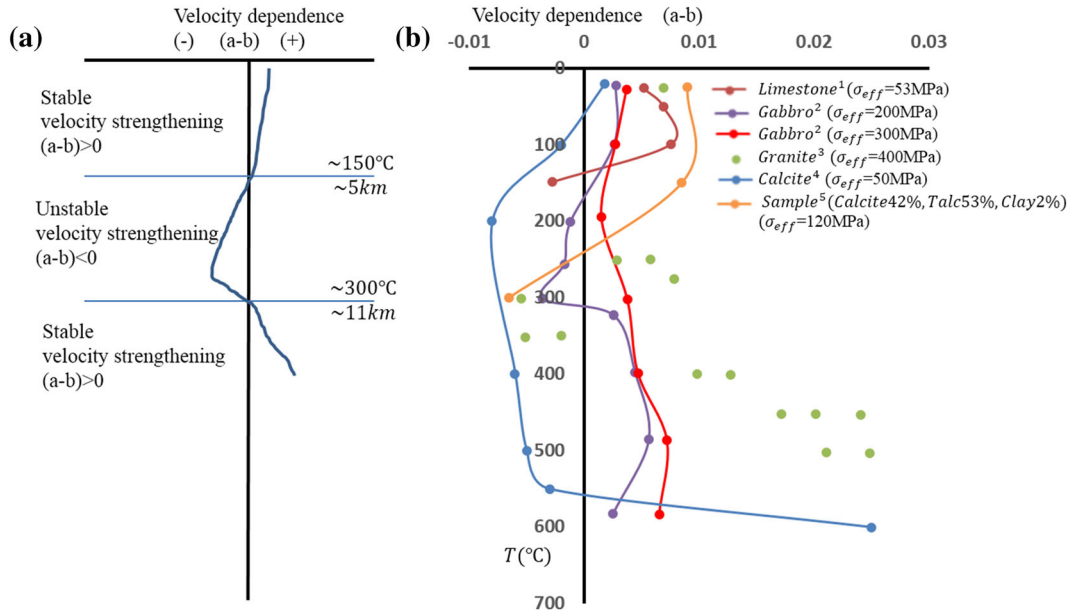

Fig. 13 Frictional parameter (a − b) as a function of temperature. **a** Fault slip behaviors change with the depth. **b** The frictional parameter (a − b) vs temperature. Data of limestone was obtained at shear velocity steps between 0.122 µm/s and 1.22 µm/s (Verberne et al. 2010). Data of gabbro was generated from the same shear velocity steps above (He et al. 2007). Data of granite was generated from shear velocity steps between 0.115 µm/s and 1.15 µm/s (Blanpied et al. 1995). Data of calcite was obtained using the shear velocity steps between 0.1 µm/s and 0.3 µm/s (Verberne et al. 2015). Data of sample (calcite 42%, talc 53%, clay 2%) was generated from shear velocity steps between 0.3 µm/s and 1 µm/s (Niemeijer and Collettini 2013)

montmorllonite (absorbing mineral) is as high as 93%, because of the decrease of absorbing mineral strength in saturate condition. In contrast, the non-absorbing minerals, e.g., quartz, keep the frictional strength after saturation. The different decreases in the friction coefficient depend on absorbing mineral content in fault gouges.

The reason for the frictional strength decreases of fault gouges with absorbing minerals, e.g., montmorllonite and kaolinite, after saturation is that the surface of sheet structure minerals attracts water molecules and a thin film of water between two adjacent sheet structure minerals determines the frictional strength (Renard and Ortoleva 1997; Moore 2004). Sakuma and Kawamura (2009) conducted molecular dynamics simulations, and concluded that the frictional strength decrease is because the sheet structure minerals absorb more water molecules. The surface cations of absorbing minerals influence the physical properties of the thin film of water (Sakuma and Kawamura 2011). Kawai et al. (2015) carried out frictional experiments on moscovite and explained the degree of the frictional strength decrease in terms of the fluid chemistry of NaCl or CsCl solutions, which directly certifies the effect of absorbed water on the frictional strength.

Minerals with sheet structure and high water-absorbing quality have been observed on the natural faults (Vrolijk 1990; Uda et al. 2001; Kuo et al. 2009; Kameda et al. 2011). Based on the above mechanisms, faults with these minerals can easily be reactivated by fluid pressure via two paths shown in Fig. 15. When fluid infiltrates to these faults, e.g., fluid injection in the oil and gas industry and pressure diffusion in reservoir dams, these faults may be reactivated due to the friction coefficient decrease. In addition, the effective stress loading on the fault decreases with increasing fluid pressure, which facilitates fault reactivation.

4.2.2 Stress corrosion

Pore water can play a two-fold role in the earthquake process, i.e., a mechanical effect as pore pressure and a chemical effect as stress-aided corrosion. There is evidence suggesting that pore water or pore pressure diffuses along pre-existing fractures and bedding

Table 2 Summary of the average coefficient of friction of fault gouges in dry and wet conditions

Fault gouges	Coefficient of friction (dry)	Coefficient of friction (wet)	Decrease percentage (%)	References
Lizardite	0.8	0.4	50	Moore (2004)
Talc	0.35	0.2	43	
Kaolinite	0.85	0.5	41	
Brucite	0.46	0.3	35	
Gibbisite	0.74	0.5	32	
Chlorite	0.68	0.48	29	
Margarite	0.82	0.6	27	
Biotite	0.46	0.35	24	
Clintonite	00.72	0.65	10	
50%Mont.50% Quartz	0.57	0.21	63	Ikari et al. (2007)
Montmorllonite	0.41	0.03	93	
Serpentine	0.66	0.51	23	Okazaki et al. (2013)
Muscovite	0.28	0.2	29	Kawai et al. (2015)

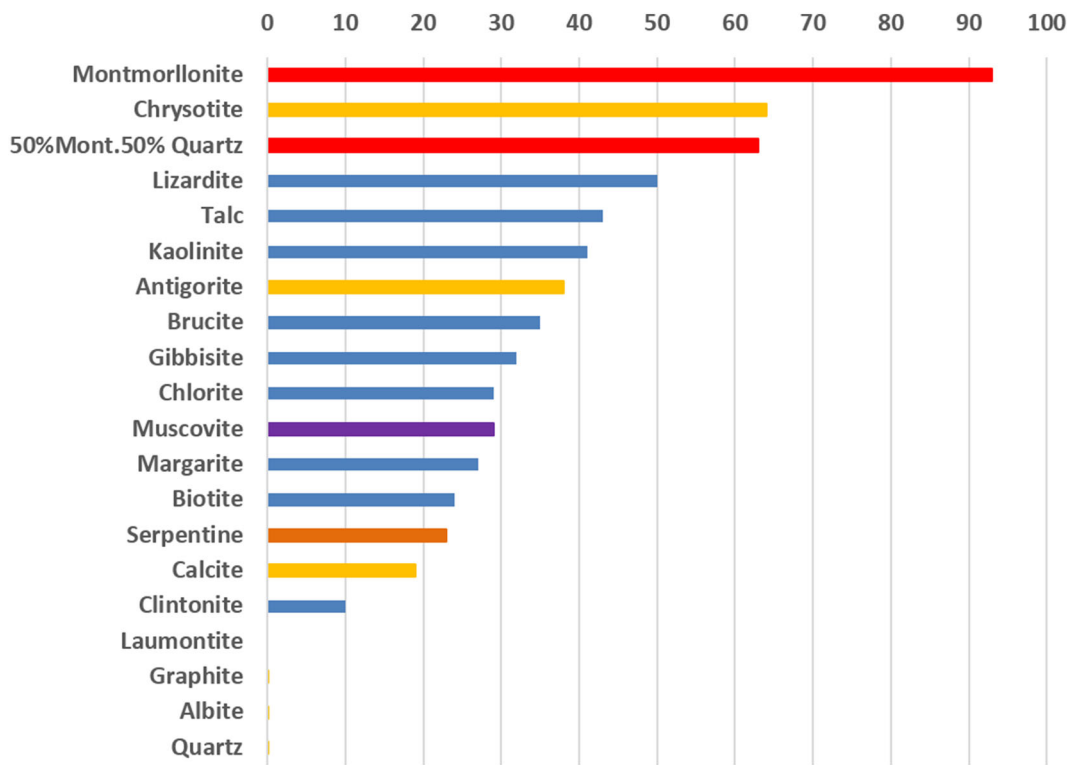

Fig. 14 Decrease percentage in friction coefficient when the gouge changes from dry to saturated conditions. The data is taken from Morrow et al. (2000) (Orange), Moore (2004) (Blue), Ikari et al. (2007) (Red), Okazaki et al. (2013) (Green), Kawai et al. (2015) (Purple)

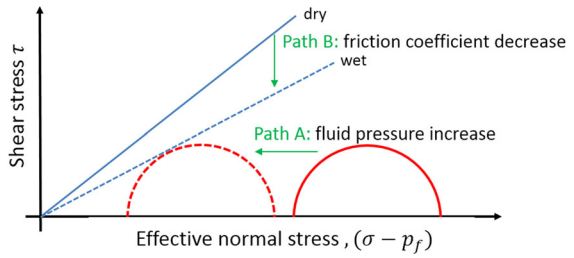

Fig. 15 Schematic representation of fault reactivation. Path A: Induced earthquakes attributed to the decreasing effective normal stress with increasing fluid pressure. Path B: Induced earthquakes due to the decrease coefficient of friction in saturated gouges with rich phyllosilicate. The critical condition is that the Mohr's envelope is tangent to the frictional slope of faults (Jaeger and Cook 1979)

planes, etc. (Witherspoon and Gale 1977), and can attribute to new crack propagation through stress corrosion (Anderson and Grew 1977). For example, injecting non-native fluids into the formation may cause geochemical alteration of fracture surfaces, thus changing the coefficient of friction on those surfaces. In the case of reduced friction, smaller seismic events would be more likely to occur (Ernest et al. 2007).

In the case of silicate rocks with water as the corrosive agent, the following stress corrosion reaction is implied (Nara et al. 2011):

$$[\mathrm{Si{-}O{-}Si}] + \mathrm{H_2O} \rightarrow 2[\mathrm{SiOH}] \quad (18)$$

This stress corrosion reaction corresponds to a chemical attack through a hydrolysis reaction of the strong siloxane [Si–O–Si] bonds at crack tips. The reaction induces bond rupture and the formation of terminal silanol [SiOH] groups with weaker bonds. This chemical reaction is facilitated by high tensile stresses at crack tips. Activation energy barriers are modified by mechanical stress levels, thus influencing chemical reaction rates in solids (Lawn 1993). Subcritical crack growth in different conditions is summarized in Table 3. As shown in Table 3, stress corrosion cracking is enhanced by the presence of water as well as temperature, because water or temperature changes the activation energy of the chemical reaction (Scholz 1972; Nara et al. 2011).

5 Statistics

Tables 4, 5 and 6 summarize induced earthquakes related to human activities. Well-documented examples of earthquake activity induced by fluid injection and extraction include earthquakes induced by waste injection in Oklahoma, USA (Keranen et al. 2013), Youngstown, USA (Kim 2013); secondary recovery of oil in Colorado, USA (Raleigh et al. 1972), West Texas, USA (Davis 1985), western Alberta, Canada (Milne 1970) and southwestern Ontario, Canada (Mereu et al. 1986); solution mining for salt in western New York, USA (Fletcher and Sykes 1977); and fluid stimulation in EGS in New Mexico, USA (Pearson 1981), Soultz-sous-Forêts, France (Cuenot et al. 2008, 2011) and Basel, Switzerland (Deichmann and Giardini 2009). The maximum magnitude of reservoir induced earthquakes, e.g., Hsinfengkiang, China in 1962, Kariba, Zambia–Zimbabwe Border in 1963, Kremasta, Greece in 1966 and Koyna, India in 1967, exceeds M 6, which is greater than earthquakes induced by fluid injection and extraction or mining.

Figure 16a shows earthquake magnitude vs frequency of reported examples of injection induced seismicity whose magnitudes range from 1.0 to 5.7. Figure 16b shows the maximum observed magnitudes for different sources of seismicity. Figure 16 reveals that among all injection induced earthquakes, the greatest one (ML 5.7) results from wastewater disposal. This is because the injection depth of waste water is much greater than other well operations such as production reservoirs, due to needs for permanent sequestration and isolation from oil/gas reservoirs and drinking-water aquifers (Rubinstein and Mahani 2015). The magnitude of fluid-injection-induced earthquakes is also found to be dependent on the net volume of injected fluid (McGarr 2014). In addition, rates of injection has influence on the size of induced seismicity (Weingarten et al. 2015).

6 Summary

This review is intended to review the induced earthquakes caused by human activities, i.e., fluid injection and extraction, reservoir impoundment and mining/rock removal, and to analyze and classify their mechanisms from a view of rock mechanics. Three fundamental mechanisms of induced earthquakes, i.e.,

Table 3 Summary of subcritical crack growth in different conditions

Sample	Condition	$K_I(10^{-5})\left(MN/m^{\frac{3}{2}}\right)$	V (m/s)	References
Inada granite	Dry	1.2	$<10^{-8}$	Kodama et al. (2003)
	Water 0 °C	1.2	1.0×10^{-7}	
	Water 40 °C	1.2	1.0×10^{-4}	
	Water 80 °C	1.2	1.0×10^{-3}	
Murata basalt	In air	1	1.0×10^{-15}	Sano and Kudo (1992)
	In water PH = 7	1	1.0×10^{-11}	
	In water PH = 3	1	1.0×10^{-13}	
	In water PH = 11	1	$1.0 \times 10^{-9.8}$	
Oshima granite	In air	1	1.0×10^{-11}	
	In water PH = 7	1	$1.0 \times 10^{-10.4}$	
	In water PH = 3	1	$1.0 \times 10^{-10.9}$	
	In water PH = 11	1	$1.0 \times 10^{-7.6}$	
Berea sandstone	Humidity (18 ~ 27%) 20 °C	0.32	1.3×10^{-7}	Nara et al. (2011)
	Humidity (54–56%) 20 °C	0.27	1.9×10^{-3}	
	Humidity (89–92%) 20 °C	0.26	7.2×10^{-2}	
Berea sandstone	Humidity (54–56%) 20 °C	0.27	3.0×10^{-6}	
	Humidity (53%) 56 °C	0.26	5.0×10^{-5}	
	Humidity (51–54%) 77 °C	0.27	1.5×10^{-5}	
Peridotite	Air 20 °C	0.95	$10^{-3.6}$	Hao et al. (2015)
	Water 20 °C	0.95	$10^{-1.6}$	
Lherzolite	Air 20 °C	0.25	10^{-3}	
	Water 20 °C	0.25	$10^{-1.6}$	
Amphibolite	Air 20 °C	0.13	$10^{-3.9}$	
	Water 20 °C	0.13	$10^{-0.6}$	

pore pressure increase, stress change and change in coefficient of friction, are summarized in details. This section presents concluding remarks and potential means and scopes to investigate the mechanism of induced earthquakes.

Induced earthquake occurs when the mechanical state of the seismogenic crust is sufficiently perturbed to cause the fault to failure. As indicated in Eq. (10), failure can occur because of the increase of shear stress loading on the fault, the reduction of fault strength due to a decrease in the normal stress, the decrease of coefficient of friction or the increase in the pore pressure.

Induced earthquakes are classified into three categories, i.e., reservoir induced earthquakes, mining induced earthquakes and fluid injection/extraction induced earthquakes. The reasons and mechanisms for those induced earthquakes are illustrated in Fig. 17. Reservoir induced earthquakes mainly result from stress change and pore pressure change. Mining induced earthquakes are mostly attributed to stress change, i.e., mechanical unloading. The main cause of fluid injection induced earthquakes is pore pressure change. The change of coefficient of friction is usually too small to induce instable slip.

The HM coupling (Fig. 18) is widely applied in the study of hydraulic fracturing and reservoir induced earthquakes. Although factors influencing the hydraulic–mechanical coupling, i.e., effective normal stress, fracture normal and shear deformation, shear strength and fracture flow, are considered, it is still not completely clear how induced earthquakes are correlated with HF coupling.

Table 4 Acknowledged cases of induced earthquake associated with well operations

Location	Injection volume (m3)	Injection rate (L/s)	Well depth (m)	Injection pressure (MPa)	Date of earthquake $(M_l)_{max}$	$(M_l)_{max}$	Type
Oklahoma USA					06-Nov-2011	5.7	Waste disposal
Rocky Mountain Arsenal, Colorado USA	620,000	7.97	3700	41.5	1967	5.5	Waste disposal
Western Alberta, Canada					8-Mar-1970	5.1	Secondary recovery
East Texas USA					17-May-2012	4.9	Waste disposal
Fashing, Texas USA					10-Oct-2011	4.8	Gas withdraw
Cogdell Canyon Reef Oil Field, West Texas			2265	21.7	Jun-1978	4.7	Secondary recovery
Arkansas USA					27-Feb-2011	4.7	Waste disposal
The Geysers field in Northern California USA		347.22	3000		1982	4.6	Geothermal
Berlin, El Salvador	300,000				16-Sep-2003	4.4	Geothermal
Permian Basin West Texas Oil Fields			3700	7	1964–1976	4.4	Secondary recovery
Snyder, Texas USA					11-Sep-2011	4.4	Secondary recovery
Youngstown Ohio USA					31-Dec-2011	4	Waste disposal
Atascosa County, South Texas			3400	7.1	Mar-1984	3.9	
Cooper Basin, Australia	20,000	48	4421		14-Nov-2003	3.7	Geothermal
Ashtabula, Ohio			1845		1987	3.6	Waste disposal
Basel Deep Heat Mining project, Switzerland	11,566	62.5		29.6	8-Dec-2006	3.4	Geothermal
Rangely, Colorado USA	9,700,000		1900	27.5	1962–1975	3.1	Secondary recovery
Soultz-sous-Foȇts, France	40,000	80	5260		10-Jun-2003	2.9	Geothermal
Sleepy Hollow Oil Field, Nebraska			1170	14.2	1979–1980	2.9	Secondary recovery
Southwestern Ontario, Canada			884		Dec-1979	2.8	Secondary recovery
Calhio, Perry, Ohio			1810	11.4	1983–1987	2.7	Waste disposal
Landau, Germany		70	3000	6	2007	2.7	Geothermal
Hellisheidi Iceland		50	2500	1.7	2003	2.4	Geothermal
the Preese Hall well, near Blackpool UK	2245		2663		2011	2.3	Secondary recovery
Rosemanowes UK		33	2500	11	1987	2	Geothermal
Bad Urach, Germany		50	4300	34	2002	1.8	Geothermal
KTBborehole, Germany		9	9100	55	1994	1.2	Geothermal
Attica-Dale, New York USA			426	5.5	1971–1977	1	Solution mining
Krafla Iceland		45	2000	0.1	Apr-2002	≤ 2	Geothermal
Fenton Hill, New Mexico	7600	26.67	2930		1979	< 1	hydraulic fracturing experiment

Table 5 Acknowledged cases of artificial water reservoir induced earthquakes

Name of the dam	Country	Height of dam (m)	Reservoir volume ($10^6 m^3$)	Year of impounding	M_L (max)	Year of largest earthquake	References
Koyna	India	103	2780	1962	6.3	1967	1, 2, 3
Kariba	Zamba–Zimbabwe	128	175,000	1958	6.2	1963	1
Kremasta	Greece	160	4750	1965	6.2	1966	1
Hsinfengkiang	China (PRC)	105	139,896	1959	6.1	1962	1
Srinagari	Thailand	140	11,750	1977	5.9	1983	4
Oroville	USA	236	4400	1967	5.7	1975	5
Marathon	Greece	67	41	1929	5.7	1938	5
Aswan	Egypt	111	164,000	1964	5.6	1981	5
Eucumbene	Australia	116	4761	1957	5	1959	5
Bhatsa	India	88	947	1981	4.9	1983	6
Kerr	USA	60	1505	1958	4.9	1971	7
Monteynard	France	155	275	1962	4.9	1963	8, 9
Shenwo	China	50	540	1972	4.8	1974	10
Canelles	Spain	150	678	1960	4.7	1964	8, 9
Danjiangkou	China	97	16,000	1967	4.7	1973	10
Dahua	China	74.5	420	1982	4.5	1993	11
Vouglans	France	130	605	1968	4.4	1971	8, 9
Clark Hill	USA	60	3517	1952	4.3	1974	12
Camarillas	Spain	49	37	1960	4.1	1964	8, 9
Manicouagan	Canada	108	10,423	1975	4.1	1975	5
Dhamni	India	59	285	1983	3.8	1994	13
Shengjiaxia	China	35	4	1980	3.6	1986	14
Talbingo	Australia	162	935	1971	3.5	1973	15, 16
Lubuge	China	103	110	1988	3.4	1988	17
Jocasse	USA	107	1431	1971	3.2	1975	18
Shuikou	China	101	2350	1993	3.2	1994	14
Zhelin	China	62	7170	1972	3.2	1972	10
Contra	Switzerland	220	86	1963	3	1965	8, 9
Kamafusa	Japan	47	45	1970	3	1970	19
Tongjiezi	China	74	30	1992	2.9	1992	20
Hunanzhen	China	129	2060	1979	2.8	1979	21
Monticello	USA	129	500	1977	2.8	1979	12, 18
Nanchong	China	45	15	1969	2.8	1970	10
Huangshi	China	40	610	1970	2.3	1974	10

1. Gupta and Rastogi (1976), 2. Gupta and Combs (1976), 3. Gupta (1983), 4.Chung and Liu (1992), 5. Packer et al. (1979), 6. Rastogi et al. (1986), 7. Simpson (1976), 8. Rothe (1970, 1973), 9. Bozovic (1974), 10. Oike and Ishikawa (1983), 11. Guang (1995), 12. Talwani (1976), 13. Rastogi et al. (1997), 14. Hu et al. (1996), 15. Soboleva and Mamadaliev (1976), 16. Muirhead et al. (1973), 17. Jiang and Wei (1995), 18. Talwani et al. (1980), 19. Suzuki (1975), 20. Guo (1994), 21. Hu et al. (1986)

As shown in Fig. 19, mining induced earthquake is usually defined as the mechanical behaviors of rock; hydraulic fracturing and reservoir induced earthquakes are affected by fluid and mechanics; and the mechanisms of geothermal induced earthquake involve the THM coupling where a number of factors,

Table 6 Acknowledged cases of mining induced earthquake

Mine	Time when seismic problem initiated	Depth (m)	Max magnitude $(M_L)_{max}$	Occurrence time of $(M_L)_{max}$
Newcastle coal mine Australia			5.6	1989
Völkershausen German		900	5.4	1989
Klerksdorp Gold mine, South Africa			5.3	2005
Welkom Gold mine, South Africa			5.2	1976
Klerksdorp District gold mine, South Africa		3000	5.2	1986
Wyoming Trona Mines USA			5.1	1995
Klerksdorp Gold mine, South Africa			4.9	2004
Zigong Salt Mine, China			4.6	1985
Lubin copper basin, Poland	1972	600	4.5	1977
Taiji coalmine, China	1970	550	4.3	2004
Chayuan coalmine, China			4.3	1987
Taiji coalmine, China	1947	200	4.2	1994
Huachu coalmine, China			4.1	1982
Carletonville gold mine, South Africa		4000	4	
Saarland coal mine, Germany			4	2008
East Rand Proprietary gold mine		3000	3.8	
Nanshan coalmine, China	1981	347	3.7	2001
Laohutai coalmine, China	1955	300	3.7	1978
Saskatchewan Potash Mine, Canada		1000	3.6	1985
Taozhuang coalmine, China	1976	450	3.6	1982
North Staffordshire Coal Field, England		1000	3.5	
Staffordshire coal mine, Britain		1000	3.5	
Sanhejian coalmine, China	1991	545	3.4	2003
Grangesberg Mines, Central Sweden		550	3.2	1974
Esterhazy Cory potash mine, Canada		7100	3.1	
Sunnyaide coalj mining district, USA		3000	2.8	
Shengli coalmine, China	1933	300	2.8	1978
Utah coal mine, USA			2.2	2000

e.g., porosity, permeability, poro-elasticity, density, viscosity, heat transport, friction heating and thermal expansion, need to be considered.

Although we have had a preliminary understanding about the mechanisms of induced earthquakes, more than one parameter, e.g., stress, temperature and pore pressure, may be involved, and those parameters may be coupled. Because of the complexity, it is necessary to adopt appropriate means and carry out further study to better understand induced earthquakes subjected to thermal, hydraulic and mechanical loadings.

Many factors, e.g., fluid, mineralogy and temperature, control the fault slip behaviors and may facilitate aseismic slip. However, there have been seismic slips occurring on or adjacent to the fault reactivated and exhibiting stable sliding (Wei et al. 2015; Guglielmi et al. 2015). There are two mechanisms for evolution from stable to unstable slip. One is

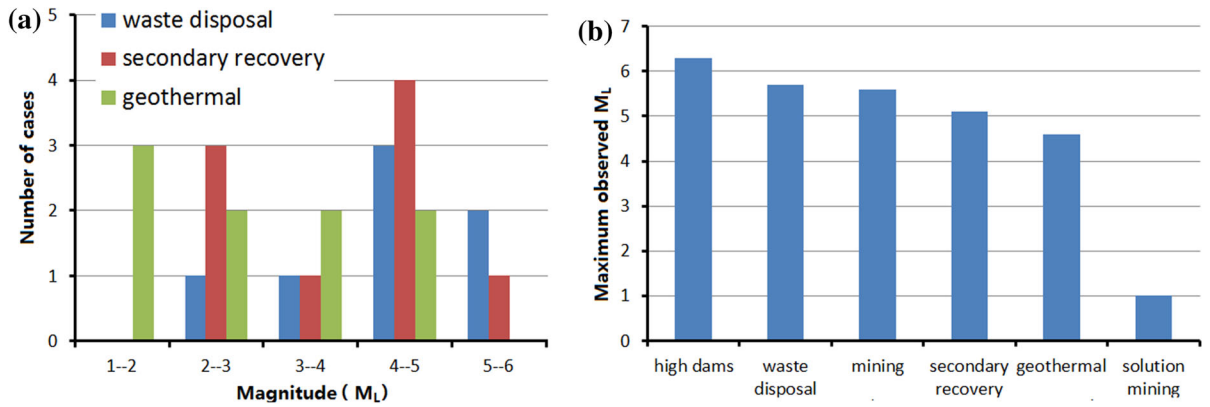

Fig. 16 Summaries of induced earthquakes. **a** Frequency vs magnitude for reported examples of injection induced seismicity. **b** Maximum observed magnitudes for different sources of seismicity. The data are taken from Tables 4, 5 and 6

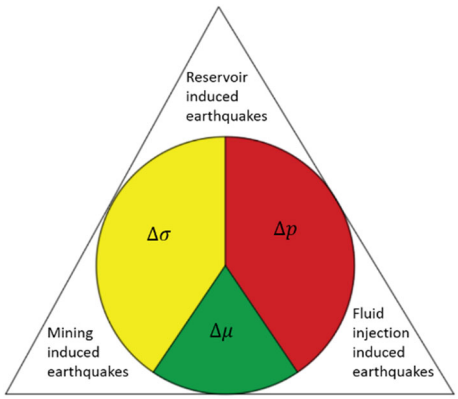

Fig. 17 Schematic diagram illustrating the major mechanisms of the reservoir, mining and fluid injection induced earthquakes

that the fault stable slip may transfer to unstable sliding if the stress, fluid pressure and temperature etc. change suddenly and dramatically. The other one is that induced earthquakes may result from static stress transfer produced by aseismic slip. Therefore, it is complicated to analyze the fault slip considering the combination of these above factors. At present, researchers pay many attentions to the whole process, i.e., the evolution from stable to unstable slip, of induced earthquakes to understand and evaluate induced earthquakes (Guglielmi et al. 2015; Scuderi and Collettini 2016; De Barros et al. 2016). Additionally, a new scheme named "cyclic hydraulic fracturing" was introduced in order to reduce induced seismicity (Zang et al. 2013). Based on the new scheme, some laboratory studies considering injection rate and rock characteristics were conducted (Zhuang et al. 2016, 2018). However, this new scheme could effectively control induced seismicity only in the stage of laboratory test and numerical analysis. To achieve these goals, further field tests, e.g., injection tests, and laboratory experiments, e.g., biaxial tests and triaxial tests, are, therefore, recommended in the future.

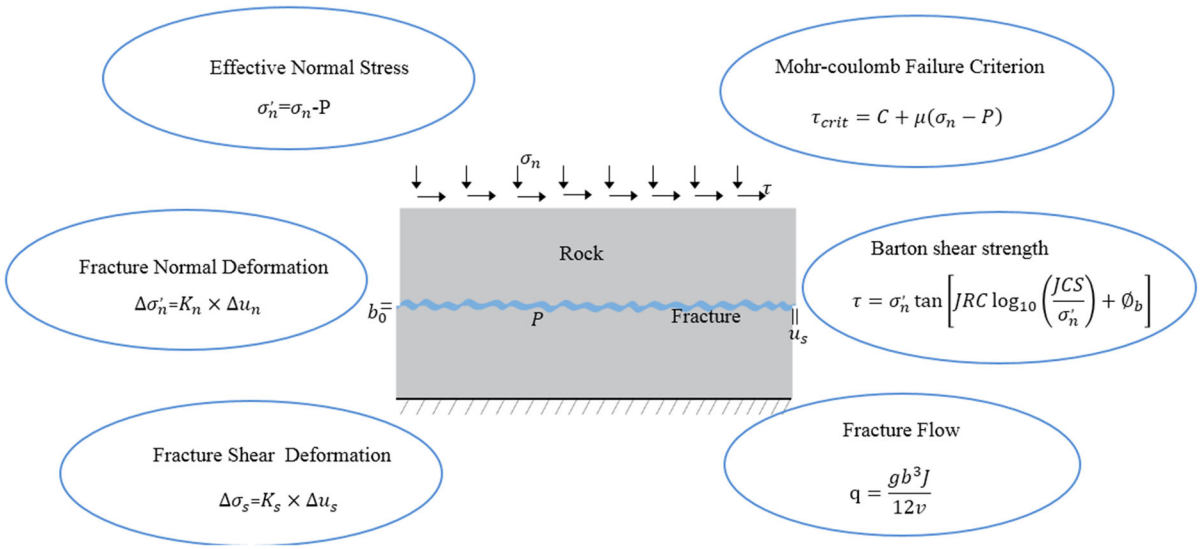

Fig. 18 Schematic diagram illustrating hydraulic–mechanical coupling in a fluid-saturated, porous-medium-like rock composed of a fracture

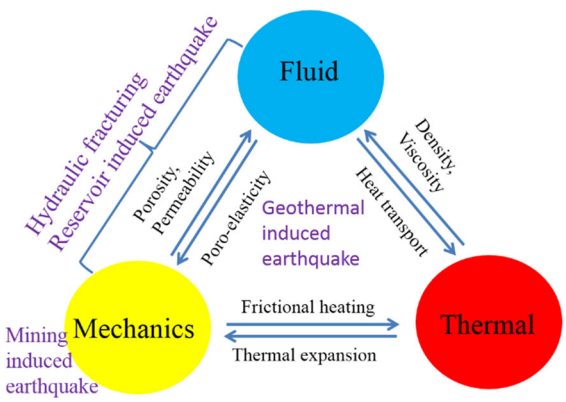

Fig. 19 Schematic diagram illustrating the THM coupling

References

Addis MA (1997) Reservoir depletion and its effect on wellbore stability evaluation. Int J Rock Mech Min Sci 34:3–4

Anderson OL, Grew PC (1977) Stress corrosion theory of crack propagation with application to geophysics. Rev Geophys Space Phys 15:77–104

Atkinson GM, Eaton DW, Ghofrani H, Walker D, Cheadle B, Schultz R, Kao H (2016) Hydraulic fracturing and seismicity in the Western Canada sedimentary basin. Seismol Res Lett 87(3):631–647

Bell JS (1990) Investigating stress regimes in sedimentary basins using information from oil industry wireline logs and drilling records. Geol Soc Lond Spec Publ 48(1):305–325

Bell ML, Nut A (1978) Strength changes due to reservoir-induced pore pressure and stresses and application to Lake Oroville. J Geophys Res 83:4469–4483

Biot MA (1941) General theory of three-dimensional consolidation. J Appl Phys 12:155–164

Blanpied ML, Lockner DA, Byerlee JD (1995) Frictional slip of granite at hydrothermal conditions. J Geophys Res Solid Earth 100(B7):13045–13064

Boucher G, Ryall A, Jones AE (1969) Earthquakes associated with underground nuclear explosions. J Geophys Res 74(15):3808–3820

Boulton C, Carpenter BM, Toy V, Marone C (2012) Physical properties of surface outcrop cataclastic fault rocks, Alpine Fault, New Zealand. Geochem Geophys Geosyst 13(1):Q01018. https://doi.org/10.1029/2011gc003872

Bozovic A (1974) Review and appraisal of case histories related to seismic effects of reservoir impounding. Eng Geol 8:9–27

Breckels IM, van Eekelen HAM (1982) Relationship between horizontal stress and depth in sedimentary basins. J Pet Technol 34:2191–2198

Bruel D (2002) Impact of induced thermal stresses during circulation tests in an engineered fractured geothermal reservoir; example of the Soultz-sous-Forets European hot fractured rock geothermal project, Rhine Graben, France. Oil Gas Sci Technol Rev IFP 57:459–470

Byerlee J (1978) Friction of rocks. In: Byerlee JD, Wyss M (eds) Rock friction and earthquake prediction. Contributions to current research in geophysics (CCRG), vol 6. Birkhäuser, Basel

Byerlee JD, Brace WF (1968) Stick slip, stable sliding, and earthquakes-effect of rock type, pressure, strain rate, and stiffness. J Geophys Res 73(18):6031–6037

Carpenter BM, Marone C, Saffer DM (2009) Frictional behavior of materials in the 3D SAFOD volume. Geophys Res Lett 36(5):277–291

Chung WY, Liu C (1992) The reservoir-associated earthquakes of April 1983 in Western Thailand: source modelling and implications for induced seismicity. PAGEOPH 138(1):17–41

Cipolla C, Maxwell S, Mack M (2012) Engineering guide to the application of microseismic interpretations. In: SPE Hydraulic Fracturing Technology Conference. https://doi.org/10.2118/152165-ms

Cuenot N, Dorbath C, Dorbath L (2008) Analysis of the microseismicity induced by fluid injections at the EGS site of Soultz-sous-Forêts (Alsace France): implications for the characterization of the geothermal reservoir properties. Pure Appl Geophys 165:797–828

Cuenot N, Frogneux M, Dorbath C, Calo M (2011) Induced microseismic activity during recent circulation tests at the EGS site of Soultz-sous-Forêts (France). In: Proceedings, thirty-sixth workshop on geothermal reservoir engineering, Stanford University, Stanford, California, January 31–February 2, 2011, SGP-TR-191

Davies R, Foulger G, Bindley A, Styles P (2013) Induced seismicity and hydraulic fracturing for the recovery of hydrocarbons. Mar Pet Geol 45:171–185

Davis SD (1985) Investigations of natural and induced seismicity in the Texas panhandle: Austin, University of Texas, M.S. thesis, p 230

De Barros L, Daniel G, Guglielmi Y, Rivet D, Caron H, Payre X, Gourlay M (2016) Fault structure, stress, or pressure control of the seismicity in shale? Insights from a controlled experiment of fluid-induced fault reactivation. J Geophys Res Solid Earth 121(6):4506–4522

De Simone S, Vilarrasa V, Carrera J, Alcolea A, Meier P (2013) Thermal coupling may control mechanical stability of geothermal reservoirs during cold water injection. Phys Chem Earth A/B/C 64:117–126

Deichmann N, Giardini D (2009) Earthquakes induced by the stimulation of an enhanced geothermal system below Basel (Switzerland). Seismol Res Lett 80(5):784–798

Deichmann N, Kraft T, Evans KF (2014) Identification of faults activated during the stimulation of the Basel geothermal project from cluster analysis and focal mechanisms of the larger magnitude events. Geothermics 52:84–97

Den Hartog SAM, Niemeijer AR, Spiers CJ (2012a) New constraints on megathrust slip stability under subduction zone P–T conditions. Earth Planet Sci Lett 353–354:240–252

Den Hartog SAM, Peach CJ, de Winter DAM, Spiers CJ, Shimamoto T (2012b) Frictional properties of megathrust fault gouges at low sliding velocities: new data on effects of normal stress and temperature. J Struct Geol 38:156–171

Dieterich JH (1978) Time-dependent friction and the mechanics of stick-slip. Pure Appl Geophys 116:790–806

Ellsworth WL (2013) Injection-induced earthquakes. Science 341(6142):1225942

Engelder T, Fischer MP (1994) Influence of poroelastic behaviour on the magnitude of minimum horizontal stress, S_h, in overpressured parts of sedimentary basins. Geology 22:949–952

Ernest LM, Roy B, Mitch S, Stephen O, Julian B, Bill S, Hiroshi A (2007) Induced seismicity associated with enhanced geothermal systems. Geothermics 36:185–222

Feng Y, Chen X, Xu XF (2014) Current status and potentials of enhanced geothermal system in China: a review. Renew Sustain Energy Rev 33:214–223

Fletcher JB, Sykes LR (1977) Earthquakes related to hydraulic mining and natural seismic activity in western New York State. J Geophys Res 82:3767–3780

Ghassemi A, Zhou X (2011) A three-dimensional thermo-poroelastic model for fracture response to injection/extraction in enhanced geothermal systems. Geothermics 40(1):39–49

Ghassemi A, Nygren A, Cheng A (2008) Effects of heat extraction on fracture aperture: a poro-thermoelastic analysis. Geothermics 37(5):525–539

Grasso J (1992) Mechanics of seismic instabilities induced by the recovery of hydrocarbons. Pure appl Geophys 139(3):507–534

Grünthal G (2014) Induced seismicity related to geothermal projects versus natural tectonic earthquakes and other types of induced seismic events in Central Europe. Geothermics 52:22–35

Guang YH (1995) Seismicity induced by cascade reservoirs in Dahan, Yantan Hydroelectric Power Stations. In: Proceedings international symposium on reservoir-induced seismicity. State Seismological Bureau, Beijing, pp 157–163

Guglielmi Y, Cappa F, Avouac JP, Henry P, Elsworth D (2015) Seismicity triggered by fluid injection-induced aseismic slip. Science 348(6240):1224–1226

Guo MK (1994) Earthquake due to the reservoir for power station at the Tangjiezi in sichuan province. Earthq Res Sichuan 2:12–23

Gupta HK (1983) Induced seismicity hazard mitigation through water level manipulation at Koyna, India: a suggestion. Bull Seismol Soc Am 73:679–682

Gupta HK (2002) A review of recent studies of triggered earthquakes by artificial water reservoirs with special emphasis on earthquakes in Koyna, India. Earth Sci Rev 58(3):279–310

Gupta HK, Combs J (1976) Continued seismic activity at the Koyna reservoir site, India. Eng Geol 10:307–313

Gupta HK, Rastogi BK (1976) Dams and earthquakes. Elsevier, Amsterdam, p 229

Hao RQ, Li JT, Cao P, Liu B, Liao J (2015) Test of subcritical crack growth and fracture toughness under water-rock interaction in three types of rocks. J Central South Univ 22(2):662–668

He C, Yao W, Wang Z, Zhou Y (2006) Strength and stability of frictional sliding of gabbro gouge at elevated temperatures. Tectonophysics 427(1–4):217–229

He C, Wang Z, Yao W (2007) Frictional sliding of gabbro gouge under hydrothermal conditions. Tectonophysics 445(3–4):353–362

He C, Tan W, Zhang L (2016) Comparing dry and wet friction of plagioclase: implication to the mechanism of frictional evolution effect at hydrothermal conditions. J Geophys Res Solid Earth 121(9):6365–6383

Hillis RR (2000) Pore pressure/stress coupling and its implications for seismicity. Explor Geophys 31:448–454

Horner RB, Hasegawa HS (1978) The seismotectonics of southern Saskatchewan. Can J Earth Sci 15:1341–1355

Hu YL, Chen XC, Zhang ZL, Ma WT, Liu ZY, Lei J (1986) Induced seismicity at Hunanzhen Reservoir, Zhejiang Province. Seismol Geol 8:1–26

Hu YL, Liu ZY, Yang QY, Chen XC, Hu P, Ma WT, Lei J (1996) Induced seismicity at Wujiangdu Reservoir, China: a case induced in Karst Area. Pure Appl Geophys 147:409–418

Ikari MJ, Saffer DM, Marone C (2007) Effect of hydration state on the frictional properties of montmorillonite-based fault gouge. J Geophys Res 112(B6):B06423. https://doi.org/10.1029/2006jb004748

Ikari MJ, Saffer DM, Marone C (2009) Frictional and hydrologic properties of clay-rich fault gouge. J Geophys Res 114(B5):B05409. https://doi.org/10.1029/2008jb006089

Ikari MJ, Marone C, Saffer DM (2010) On the relation between fault strength and frictional stability. Geology 39(1):83–86

Jacob CE (1940) On the flow of ground water in a elastic artesian aquifer. Trans Am Geophys Union 22:783–787

Jaeger CJ, Cook NGW (1979) Fundamentals of rock mechanics: London, Methuen, p 593

Jeanne P, Rutqvist J, Dobson PF, Walters M, Hartline C, Garcia J (2014) The impacts of mechanical stress transfers caused by hydromechanical and thermal processes on fault stability during hydraulic stimulation in a deep geothermal reservoir. Int J Rock Mech Min Sci 72:149–163

Jiang QH, Wei ZS (1995) Researches on seismicity induced by Lubuge Reservoir in Yunan Province, China. In: Proceedings international symposium on reservoir-induced seismicity, Beijing, pp 197–204

Kameda J, Yamaguchi A, Saito S, Sakuma H, Kawamura K, Kimura G (2011) A new source of water in seismogenic subduction zones. Geophys Res Lett 38(22):L22306. https://doi.org/10.1029/2011gl048883

Kawai K, Sakuma H, Katayama I, Tamura K (2015) Frictional characteristics of single and polycrystalline muscovite and influence of fluid chemistry. J Geophys Res Solid Earth. 120(9):6209–6218

Keranen KM, Savage HM, Abers GA, Cochran ES (2013) Potentially induced earthquakes in Oklahoma, USA: links between wastewater injection and the 2011 Mw 5.7 earthquake sequence. Geology 41(6):699–702

Keranen KM, Weingarten M, Abers GA, Bekins BA, Ge S (2014) Sharp increase in central Oklahoma seismicity since 2008 induced by massive wastewater injection. Science 345(6195):448–451

Kim WY (2013) Induced seismicity associated with fluid injection into a deep well in Youngstown, Ohio. J Geophys Res 118(7):3506–3518

Kodaira S, Iidaka T, Kato A, Park J-O, Iwasaki T, Kaneda Y (2004) High pore fluid pressure may cause silent slip in the Nankai Trough. Science 304(5675):1295–1298

Kodama N, Fujii Y, Fujita Y, Ishijima Y (2003) Effect of temperature on deformation and failure behaviors of inada granite and shirahama sandstone in water. Shigen-to-Sozai 119(8):461–468

Kohl T, Evans KF, Hopkirk RJ, Rybach L (1995) Coupled hydraulic, thermal and mechanical considerations for the simulation of hot dry rock reservoirs. Geothermics 24(3):345–359

Kohli AH, Zoback MD (2013) Frictional properties of shale reservoir rocks. J Geophys Res Solid Earth 118(9):5109–5125

Kolditz O, Clauser C (1998) Numerical simulation of flow and heat transfer in fractured crystalline rocks: application to the hot dry rock site in Rosemanowes (UK). Geothermics 27(1):1–23

Kuo L-W, Song S-R, Yeh E-C, Chen H-F (2009) Clay mineral anomalies in the fault zone of the Chelungpu Fault, Taiwan, and their implications. Geophys Res Lett 36(18):L18306. https://doi.org/10.1029/2009gl039269

Lawn BR (1993) Fracture of brittle solids, 2nd edn. Cambridge University Press, Cambridge

Marone C, Raleigh CB, Scholz CH (1990) Frictional behavior and constitutive modeling of simulated fault gouge. J Geophys Res Solid Earth 95(B5):7007–7025

Maxwell SC, Shemeta J, Campbell E, Quirk D (2008) Microseismic deformation rate monitoring. In: SPE Annual Technical Conference and Exhibition. https://doi.org/10.2118/116596-ms

McClure MW, Horne RN (2011) Investigation of injection-induced seismicity using a coupled fluid flow and rate/state friction model. Geophysics 76(6):181–198

McClure MW, Horne RN (2014) Correlations between formation properties and induced seismicity during high pressure injection into granitic rock. Eng Geol 175:74–80

McDermott C, Randriamanjatosoa ARL, Tenzer H, Kolditz O (2006) Simulation of heat extraction from crystalline rocks: the influence of coupled processes on differential reservoir cooling. Geothermics 35:321–344

McGarr A (1976) Seismic moment and volume change. J Geophys Res 81(8):1487–1494

McGarr A (2014) Maximum magnitude earthquakes induced by fluid injection. J Geophys Res Solid Earth 119(2):1008–1019

McGarr A, Simpson D (1997) Keynote lecture: a broad look at induced and triggered seismicity, ''Rockbursts and seismicity in mines''. In: Gibowicz SJ, Lasocki S (eds) Proceedings of 4th International on rockbursts and seismicity in mines, Poland, 11–14 August, 1997

Mereu RF, Brunet J, Morrissey K, Price B, Yapp A (1986) A study of the microearthquakes of the Gobles oil field area of southwestern Ontario. Bull Seismol Soc Am 76:1215–1223

Milne WG (1970) The Snipe Lake, Alberta earthquake of March 8, 1970. Can J Earth Sci 7:1564–1567

Moore DE (2004) Crystallographic controls on the frictional behavior of dry and water-saturated sheet structure minerals. J Geophys Res 109(B3):B03401. https://doi.org/10.1029/2003jb002582

Moreno M, Haberland C, Oncken O, Rietbrock A, Angiboust S, Heidbach O (2014) Locking of the Chile subduction zone controlled by fluid pressure before the 2010 earthquake. Nat Geosci 7(4):292–296

Morrow CA, Moore DE, Lockner DA (2000) The effect of mineral bond strength and adsorbed water on fault gouge frictional strength. Geophys Res Lett 27(6):815–818

Mossop A, Segall P (1997) Subsidence at The Geysers geothermal field, California from a comparison of GPS and leveling surveys. Geophys Res Lett 24:1839–1842

Muirhead RJ, Cleary JR, Simpson DW (1973) Seismic activity associated with the filling of Talbingo Reservoir. In:

International colloquium on seismic effects of reservoir impounding, March 1973. Royal Society, London, p 17 (**summaries**)

Nara Y, Morimoto K, Yoneda T, Hiroyoshi N, Kaneko K (2011) Effects of humidity and temperature on subcritical crack growth in sandstone. Int J Solids Struct 48(7–8):1130–1140

National Research Council (2012) Induced seismicity potential in energy technologies. National Academies Press, Washington, D.C.

Niemeijer AR, Collettini C (2013) Frictional properties of a low-angle normal fault under in situ conditions: thermally-activated velocity weakening. Pure Appl Geophys 171(10):2641–2664

Oike K, Ishikawa Y (1983) Induced earthquakes associated with large reservoirs in China. Chin Geophys II 2:383–403

Okazaki K, Katayama I, Takahashi M (2013) Effect of pore fluid pressure on the frictional strength of antigorite serpentinite. Tectonophysics 583:49–53

Packer DR, Cluff LS, Knuepfer PL, Withers RJ (1979) A study of reservoir induced seismicity. Woodward-Clyde consultants, U.S.A. U.S. Geol. Surv. Contract 14-08-0001-16809

Pearson C (1981) The relationship between microseismicity and high pore pressures during hydraulic stimulation experiments in low permeability granitic rocks. J Geophys Res 86:7855–7864

Porsani JL, Sauck WA, Júnior Abad O S (2006) GPR for mapping fractures and as a guide for the extraction of ornamental granite from a quarry: a case study from southern Brazil. J Appl Geophys 58(3):177–187

Raleigh CB, Healy JH, Bredehoeft JD (1972) Faulting and crustal stress at Rangely, Colorado. In: Heard HC, Borg IY, Carter NL, Raleigh CB (eds) Flow and fracture of rocks. American Geophysical Union, Washington, D.C.

Rastogi BK, Chadha RK, Raju IP (1986) Seismicity near Bhatsa reservoir, Maharashtra, India. Phys Earth Planet Inter 44:179–199

Rastogi BK, Mandal P, Kumar N (1997) Seismicity around Dhamni dam, Maharashtra, India. Pure Appl Geophys 150(3/4):493–509

Renard F, Ortoleva P (1997) Water films at grain-grain contacts: Debye-Hückel, osmotic model of stress, salinity, and mineralogy dependence. Geochim Cosmochim Acta 61(10):1963–1970

Richardson E, Jordan T (2002) Seismicity in deep gold mines of South Africa: implications for tectonic earthquakes. Bull Seismol Soc Am 92(5):1766–1782

Rothe JP (1970) The seismic artificials (man-made earthquakes). Tectonophysics 9:215–238

Rothe JP (1973) A geophysics report. In: Ackermann WC, White GF, Worthington EB (eds) Man-made lakes: their problems and environmental effects. Geophysical Monograph Series, vol 17. American Geophysical Union, pp 441– 454

Rubinstein JL, Mahani AB (2015) Myths and facts on wastewater injection, hydraulic fracturing, enhanced oil recovery, and induced seismicity. Seismol Res Lett 86(4):1060–1067

Ruina A (1983) Slip instability and state variable friction laws. J Geophys Res 88(B12):10359–10370

Rutledge JT, Phillips WS (2003) Hydraulic stimulation of natural fractures as revealed by induced microearthquakes, Carthage Cotton Valley gas field, east Texas. Geophysics 68:441–452

Rutqvist J, Freifeld B, Min KB, Elsworth D, Tsang Y (2008) Analysis of thermally induced changes in fractured rock permeability during 8 years of heating and cooling at the Yucca Mountain Drift Scale Test. Int J Rock Mech Min Sci 45(8):1373–1389

Sakuma H, Kawamura K (2009) Structure and dynamics of water on muscovite mica surfaces. Geochim Cosmochim Acta 73(14):4100–4110

Sakuma H, Kawamura K (2011) Structure and dynamics of water on Li^+-, Na^+-, K^+-, Cs^+-, $H3O^+$-exchanged muscovite surfaces: a molecular dynamics study. Geochim Cosmochim Acta 75(1):63–81

Salz LB (1977) Relationship between fracture propagation pressure and pore pressure. Soc Pet Eng Pap SPE 6870:1–9

Sano O, Kudo Y (1992) Relation of fracture resistance to fabric for granitic rocks. Pure Appl Geophys 138:657–677

Santarelli FJ, Tronvoll JT, Svennekjaier M, Skeie H, Henriksen R, Bratli RK (1998) Reservoir stress path: the depletion and the rebound. In: Proceedings of the SPE/ISRM conference on rock mechanics and petroleum engineering, Trondheim. Paper SPE 47350

Scholz CH (1972) Static fatigue of quartz. J Geophys Res 77(11):2104–2114

Scholz CH (1998) Earthquakes and friction laws. Nature 391(6662):37–42

Scholz CH (2002) The mechanics of earthquakes and faulting, 2nd edn. Cambridge University Press, Cambridge

Schulz S, Burford RO, Mavko B (1983) Influence of seismicity and rainfall on episodic creep on the San Andreas fault system in central California. J Geophys Res Solid Earth 88(B9):7475–7484

Scuderi MM, Collettini C (2016) The role of fluid pressure in induced vs. triggered seismicity: insights from rock deformation experiments on carbonates. Sci Rep 6:24852

Seeber L, Armbruster JG, Kim WY (2004) A fluid-injection-triggered earthquake sequence in Ashtabula, Ohio: implications for seismogenesis in stable continental regions. Bull Seismol Soc Am 94:76–87

Segall P (1989) Earthquakes triggered by fluid extraction. Geology 17(10):942–946

Segall P, Fitzgerald SD (1998) A note on induced stress changes in hydrocarbon and geothermal reservoirs. Tectonophysics 289:117–128

Segall P, Lu S (2015) Injection-induced seismicity: poroelastic and earthquake nucleation effects. J Geophys Res Solid Earth 120(7):5082–5103

Segall P, Grasso JR, Mossop A (1994) Poroelastic stressing and induced seismicity near the Lacq gas field, Southwestern France. J Geophys Res Solid Earth 99(B8):15423–15438

Segall P, Rubin AM, Bradley AM, Rice JR (2010) Dilatant strengthening as a mechanism for slow slip events. J Geophys Res Solid Earth 115(B12):B12305. https://doi.org/10.1029/2010jb007449

Shapiro SA, Dinske C (2009) Fluid-induced seismicity: pressure diffusion and hydraulic fracturing. Geophys Prospect 57(2):301–310. https://doi.org/10.1029/2005gl024659

Shapiro SA, Dinske C, Rothert E (2006) Hydraulic-fracturing controlled dynamics of microseismic clouds. Geophys Res

Lett 33(14):L14312. https://doi.org/10.1029/2006gl026365
Shimamoto T, Logan JM (1981) Effects of simulated fault gouge on the sliding behavior of Tennessee sandstone: nonclay gouges. J Geophys Res Solid Earth 86(B4):2902–2914
Simpson DW (1976) Seismicity changes associated with reservoir loading. Eng Geol 10:123–150
Simpson DW (1986) Triggered earthquakes. Ann Rev Earth Planet Sci 14:21–42
Soboleva OV, Mamadaliev UA (1976) The influence of the Nurek Reservoir on local earthquake activity. Eng Geol 10:293–305
Summers R, Byerlee J (1977) A note on the effect of fault gouge composition on the stability of frictional sliding. Int J Rock Mech Min Sci Geomech Abstr 14(3):155–160
Suzuki Z (1975) Induced seismicity at Kamafusa Dam, Japan. In: Paper presented at the 1st international symposium on induced seismicity, Banff, September 15–19, 1975
Talwani P (1976) Earthquakes associated with Clark Hill Reservoir, South Carolina—a case of induced seismicity. Eng Geol 10(2–4):239–253
Talwani P, Rastogi BK, Stevenson D (1980) Induced seismicity and earthquake prediction studies in South Carolina. In: 10th Technical report, U.S. geological survey
Tembe S, Lockner DA, Wong TF (2010) Effect of clay content and mineralogy on frictional sliding behavior of simulated gouges: binary and ternary mixtures of quartz, illite, and montmorillonite. J Geophys Res Solid Earth 115(B3):B03416. https://doi.org/10.1029/2009jb006383
Terzaghi K (1923) Die Berechnung der Durchlässigkeitziffer des Tones aus dem Verlauf der hydrodynamischen Spannungs-erscheinungen. Akad Wissensch Wien Sitzungsber Math-naturwissensch Klasse IIa 142(3/4):125–138
Teufel LW, Rhett DW, Farrell HE (1991) Effect of reservoir depletion and pore pressure drawdown on in situ stress and deformation in the Ekofisk field, North Sea. American Rock Mechanics Association, Alexandria
Tingay MRP, Hillis RR, Morley CK, Swarbrick RE, Okpere EC (2003) Pore pressure/stress coupling in Brunei Darussalam—implications for shale injection. Geol Soc Lond Spec Publ 216:369–379
Uda SI, Lin A, Takemura K (2001) Crack-filling clays and weathered cracks in the DPRI 1800 m core near the Nojima Fault, Japan: evidence for deep surface-water circulation near an active fault. Island Arc 10(3–4):439–446
Van Poollen HK, Hoover DB (1970) Waste disposal and earthquakes at the rocky mountain arsenal, Derby, Colorado. J Pet Technol 22(8):983–993
Van Wees JD, Buijze L, Van Thienen-Visser K, Nepveu M, Wassing BBT, Orlic B, Fokker PA (2014) Geomechanics response and induced seismicity during gas field depletion in the Netherlands. Geothermics 52:206–219
Verberne BA, He C, Spiers CJ (2010) frictional properties of sedimentary rocks and natural fault gouge from the longmen shan fault zone, Sichuan, China. Bull Seismol Soc Am 100(5B):2767–2790
Verberne BA, Niemeijer AR, De Bresser JHP, Spiers CJ (2015) Mechanical behavior and microstructure of simulated calcite fault gouge sheared at 20–600 degrees C: implications for natural faults in limestones. J Geophys Res Solid Earth 120(12):8169–8196
Vrolijk P (1990) On the mechanical role of smectite in subduction zones. Geology 18(8):703–707
Vulgamore T, Clawson T, Pope C, Wolhart S, Machovoe S, Waltman C (2007) Applying hydraulic fracture diagnostics to optimize stimulations in the woodford shale. In: Proceedings of SPE Annual Technical Conference and Exhibition. https://doi.org/10.2523/110029-ms
Wei S, Avouac JP, Hudnut KW, Donnellan A, Parker JW, Graves RW, Eneva M (2015) The 2012 Brawley swarm triggered by injection-induced aseismic slip. Earth Planet Sci Lett 422:115–125
Weingarten M, Ge S, Godt JW, Bekins BA, Rubinstein JL (2015) High-rate injection is associated with the increase in U.S. mid-continent seismicity. Science 348(6241):1336–1340
Whitehead WS, Hunt ER, Holditch SA (1987)The effects of lithogy and reservoir pressure on the in situ stress in the Waskom (Travis Peak) Field. Society of Petroleum Engineers. https://doi.org/10.2118/16403-MS
Witherspoon PA, Gale JE (1977) Mechanical and hydraulic properties of rocks related to induced seismicity. Eng Geol I1:23–55
Wolhart SL, Harting TA, Dahlem JE, Young TJ, Mayerhofer MJ, Lolon EP (2005) Hydraulic fracture diagnostics used to optimize development in the Jonah field. https://doi.org/10.2118/102528-ms
Woodland DC, Bell JS (1989) In situ stress magnitudes from mini-frac record in western Canada. J Can Pet Technol 28(5):22–31
Yamashita T (1999) Pore creation due to fault slip in a fluid-permeated fault zone and its effect on seismicity: generation mechanism of earthquake swarm. Pure Appl Geophys 155(2):625–647
Yerkes RF, Ellsworth WL, Tinsley JC (1983) Triggered reverse fault and earthquake due to crustal unloading, northwest Transverse Ranges. Calif Geol 11(5):287–291
Yi LX, Zhao D, Liu CL (2012) Preliminary study of reservoir-induced seismicity in the three Gorges reservoir, China. Seismol Res Lett 83(5):806–814
Ying WWL (2010) Laboratory simulation of reservoir-induced seismicity. Ph.D. thesis, University of Toronto, Toronto
Zang A, Yoon JS, Stephansson O, Heidbach O (2013) Fatigue hydraulic fracturing by cyclic reservoir treatment enhances permeability and reduces induced seismicity. Geophys J Int 195:1282–1287
Zhuang L, Kim KY, Jung SG, Diaz M, Min KB, Park S, Zang A, Stephansson O, Zimmermann G, Yoon JS (2016) Laboratory study on cyclic hydraulic fracturing of Pocheon granite. In: Proceedings of the 50th US rock mechanics/geomechanics symposium, Houston, 26–29 June 2016, ARMA 16–163
Zhuang L, Kim KY, Jung SG, Diaz M, Min KB (2018) Effect of water infiltration, injection rate and anisotropy on hydraulic fracturing behavior of granite. Rock Mech Rock Eng. https://doi.org/10.1007/s00603-018-1431-3